

Ozone profile and tropospheric ozone retrievals from the Global Ozone Monitoring Experiment: Algorithm description and validation

X. Liu, K. Chance, C. E. Sioris, R. J. D. Spurr,¹ T. P. Kurosu, and R. V. Martin²

Atomic and Molecular Physics Division, Harvard-Smithsonian Center for Astrophysics, Cambridge, Massachusetts, USA

M. J. Newchurch

Atmospheric Science Department, University of Alabama, Huntsville, Alabama, USA

Received 18 May 2005; revised 4 August 2005; accepted 1 September 2005; published 29 October 2005.

[1] Ozone profiles are derived from back scattered radiance spectra in the ultraviolet (289–339 nm) measured by the Global Ozone Monitoring Experiment (GOME) using the optimal estimation technique. Tropospheric Column Ozone (TCO) is directly derived using the known tropopause to divide the stratosphere and troposphere. To optimize the retrieval and improve the fitting precision needed for tropospheric ozone, we perform extensive wavelength and radiometric calibrations and improve forward model inputs. The a priori influence of retrieved TCO is $\sim 15\%$ in the tropics and increases to $\sim 50\%$ at high latitudes. The dominant error terms are the smoothing errors, instrumental random-noise errors, and systematic temperature errors. We compare our GOME retrievals with Earth-Probe Total Ozone Mapping Spectrometer (TOMS) Total column Ozone (TO), Dobson/Brewer (DB) TO, and ozonesonde TCO at 33 World Ozone and Ultraviolet Radiation Data Centre (WOUDC) stations between 71°S and 75°N during 1996–1999. The mean biases with TOMS and DB TO are within 6 DU (2%, 1 DU = 2.69×10^{16} molecules cm^{-2}) at most of the stations. The retrieved Tropospheric Column Ozone (TCO) captures most of the temporal variability in ozonesonde TCO; the mean biases are mostly within 3 DU (15%) and the standard deviations (1σ) are within 3–8 DU (13–27%). We also compare our retrieved ozone profiles above ~ 15 km against Stratospheric Aerosol and Gas Experiment II measurements from 1996 to 1999. The mean biases and standard deviations are usually within 15%.

Citation: Liu, X., K. Chance, C. E. Sioris, R. J. D. Spurr, T. P. Kurosu, R. V. Martin, and M. J. Newchurch (2005), Ozone profile and tropospheric ozone retrievals from the Global Ozone Monitoring Experiment: Algorithm description and validation, *J. Geophys. Res.*, 110, D20307, doi:10.1029/2005JD006240.

1. Introduction

[2] The global distribution of vertical ozone profiles is essential to understand the physical and chemical processes in the atmosphere, track stratospheric ozone depletion and tropospheric pollution, improve forecasting the Ultraviolet (UV) index, and estimate climate forcing from ozone. Since the late 1970s, the global distribution of Total column Ozone (TO) has been routinely monitored from Total Ozone Mapping Spectrometer (TOMS), Solar Backscattered Ultraviolet (SBUV), and SBUV/2 instruments. Because SBUV and SBUV/2 measure backscattered radiances at 12 wavelengths with band widths of ~ 1.1 nm from 252 to 340 nm, vertical ozone information can be derived in the stratosphere above ~ 25 km [Bhartia *et al.*, 1996]. The Global Ozone Monitoring Experiment (GOME) was

launched in 1995 on the European Space Agency's (ESA) second Earth Remote Sensing (ERS-2) satellite to measure backscattered radiance spectra from the Earth's atmosphere in the wavelength range of 240–790 nm [ESA, 1995]. Observations with moderate spectral resolution of 0.2–0.4 nm and high signal to noise ratio in the Hartley (200–320 nm), Huggins (320–350 nm), and Chappuis (400–700 nm) bands make it possible to retrieve the vertical distribution of ozone in the stratosphere as well as in the troposphere [Chance *et al.*, 1997].

[3] In recent years, several algorithms have been developed to retrieve ozone profiles from GOME data [Munro *et al.*, 1998; Hoogen *et al.*, 1999; Hasekamp and Landgraf, 2001; van der A *et al.*, 2002; Müller *et al.*, 2003]. Except for the statistical neural network approach by Müller *et al.* [2003], the other algorithms are physically based and require minimizing the differences between radiances simulated with radiative transfer models and measured radiances. Among the physically-based algorithms, Hasekamp and Landgraf [2001] use Phillips-Tikhonov regularization, which does not need climatological a priori profile information but uses the first-derivative of the profile with

¹Also at RT Solutions, Inc., Cambridge, Massachusetts, USA.

²Also at Department of Physics and Atmospheric Science, Dalhousie University, Halifax, Nova Scotia, Canada.

Table 1. List of Ozonesonde Stations, Ozonesonde Type (e.g., Electrochemical Cell (ECC), Brewer-Mast (BM), Carbon Iodine (CI)), Time Period, the Availability and Type (D, Dobson; B, Brewer) of TO Measurements, and the Number of Collocated Profiles (C) and Comparisons With TOMS TO (T), Ground-Based TO (DB), and Ozonesonde Tropospheric Column Ozone (ST)

Station	Lat., °	Lon., °	Alt., m	Type	Data Period	TO	Number of Profiles			
							C	T	DB	ST
Resolute	74.7	-95.0	40	ECC	96-99	B	82	45	36	27
Scoresbysund	70.5	-22.0	128	ECC	96-99	B	99	38		43
Sodankylä	67.4	26.7	179	ECC	96-98	B	119	60	70	69
Churchill	58.7	-94.0	35	ECC	96-99	B	207	95	62	48
Valentia	51.9	-10.2	14	ECC	96-99	B	100	67	44	37
Hohenpeißenberg	47.9	11.0	975	BM	96-99	D	846	606	280	228
Payerne	46.5	6.6	491	BM	96-99	D	588	433		304
Boulder ^a	40.0	-105.3	1689	ECC	96-99	D	356	268	166	96
Ankara	40.0	32.9	891	ECC	96-99	D	65	49		24
Wallop Island	37.9	-75.5	13	ECC	96-99	D	291	229	120	121
Tateno	36.0	140.1	31	CI	96-99	D	383	259	181	101
Kagoshima	31.6	130.7	157	CI	96-99	D	289	203	124	64
Santa Cruz	28.4	-16.2	36	ECC	96,99	D	121	85		56
Naha	26.2	127.7	27	CI	96-99	D	258	174	98	54
Hilo ^a	19.6	-155.1	11	ECC	96-99	D ^b	310	256	121	53
Paramaribo ^c	5.8	-55.2	22	ECC	99	D	20	19		17
Kaashidhoo ^c	5.0	73.5	1	ECC	99	D	48	46		43
Kuala Lumpur ^c	2.7	101.7	17	ECC	98-99	D	55	38		18
San Cristobal ^c	-0.9	-89.6	8	ECC	98-99	D	77	68		30
Nairobi	-1.3	36.8	1745	ECC	98-99	D	130	118	48	37
Java ^d	-7.6	112.7	50	CI/ECC	96-99	D	158	116		31
Ascension Island	-8.0	-14.4	91	ECC	97-99	D	142	132		64
American Samoa	-14.2	-170.6	82	ECC	96-99	D	309	229	67	54
Tahiti	-18.0	-149.0	2	ECC	96-99	D	278	222		52
La Réunion ^c	-21.1	55.5	24	ECC	98-99	D	107	102		31
Irene	-25.5	28.2	1524	ECC	98-99	D	37	15	16	12
Easter Island	-27.2	-109.4	62	ECC	96-97	D	116	70		19
Laverton	-37.9	144.8	21	ECC	96-98	D ^e	147	110	78	34
Lauder	-45.0	169.7	370	ECC	96-99	D	372	304	183	94
Macquarie Island	-54.5	159.0	6	ECC	97-99	D	169	140	113	55
Marambio	-64.2	-56.1	196	ECC	96-98	D	43	19	13	25
Syowa	-69.0	39.6	42	CI	96-99	D	130	53	51	22
Neumayer	-70.7	-8.2	21	ECC	96-99	D	196	43		26

^aOzonesonde data at Boulder and Hilo are obtained from CMDL data archive (<http://www.cmdl.noaa.gov/infodata/ftpdata.html>).

^bThe TO is from a close station Mauna Loa (19.5°N, 155.6°E).

^cOzonesonde data are obtained from Southern Hemisphere Additional Ozonesonde (SHADOZ) data archive (<http://croc.gsfc.nasa.gov/shadoz>) [Thompson *et al.*, 2003a].

^dThe measurements at Java are obtained from Fujiwara *et al.* [2000] before 1998 and from SHADOZ data archive since 1998. The ozonesonde type was CI before 7 August 1999 and was switched to ECC since then.

^eThe TO is measured at a close station Melbourne (37.8°S, 145.0°E).

respect to altitude to constrain the solution; the other three algorithms are based on the Optimal Estimation (OE) inversion technique [Rodgers, 2000], which requires a priori climatology to stabilize and regularize the solution. Ozone profile retrievals from GOME spectra require better wavelength and radiometric calibration of measurements than trace gas slant column retrievals [van der A *et al.*, 2002]. Because ozone information is contained in several GOME bands, consistent calibration across different bands is critical in the retrieval. Each of the physically-based algorithms either uses only subsets of the spectral pixels from 265 to 340 nm or performs empirical corrections to GOME radiance spectra, indicating calibration problems in GOME data as well as the importance of calibrations.

[4] High fitting precision (e.g., <0.3% or better) is needed to extract useful tropospheric ozone information from the temperature-dependent Huggins bands [Chance *et al.*, 1997; Munro *et al.*, 1998]. In addition to radiometric and wavelength calibrations to GOME level-1 data, accurate modeling of the atmosphere, including Ring effect, clouds, aerosols, and temperature profiles, and the high-quality ozone cross sections, is very important in order to reduce

the fitting residuals. The accuracy of the temperature profiles used will directly affect the spectral fitting in the Huggins bands. Tropospheric UV-absorbing aerosols such as dust and carbonaceous aerosols from biomass burning have been found to affect the retrieved TOMS TO by up to 10% [Torres and Bhartia, 1999] and also affect the ozone profile retrievals from radiance spectra. Incorrect assignment of cloud information (e.g., cloud fraction, cloud-top pressure) will affect the retrieved TO and tropospheric ozone, as demonstrated by a number of studies [Thompson *et al.*, 1993; Hsu *et al.*, 1997; Koелеmeijer and Stammes, 1999; Newchurch *et al.*, 2001; Liu *et al.*, 2003, 2004]. The Ring effect, the filling-in of solar Fraunhofer lines and telluric absorption structures in the UV/visible due to inelastic Rotational Raman Scattering (RRS) by N₂ and O₂ molecules, is an important source of interference that must be properly taken into account in trace gas retrievals from remote sensing radiance spectra [Chance and Spurr, 1997; Vountas *et al.*, 1998; Storis and Evans, 2000].

[5] In this study, we perform detailed wavelength and radiometric calibrations on GOME level-1 data, improve the forward model inputs to radiative transfer simulations, and

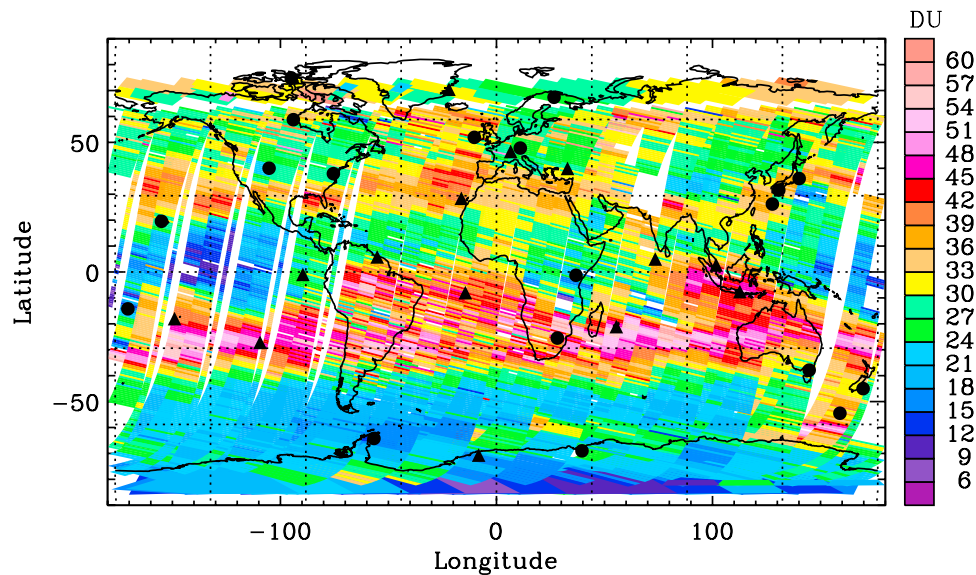


Figure 1. Three-day composite global map of tropospheric column ozone on 22–24 October 1997. The symbols indicate ozonesonde stations (circles) with and without (triangles) Dobson or Brewer total ozone observations.

derive ozone profiles and Tropospheric Column Ozone (TCO) from GOME sun-normalized ultraviolet radiances with the OE technique. We validate our retrievals against TOMS and Dobson/Brewer (DB) TO measurements, ozonesonde TCO and Stratospheric Aerosol and Gas Experiment II (SAGE-II) profiles. The paper is organized as follows. Section 2 describes the GOME data and the correlative data used for intercomparison. In section 3, we give a detailed description of the ozone profile retrieval algorithm, retrieval characterization, and error analysis. Section 4 shows examples of retrieved ozone profiles and global distribution of TCO. In section 5, we present the comparison with correlative measurements, which also serves to assess the accuracy of our retrievals. Section 6 summarizes this study.

2. Instruments and Data

2.1. GOME

[6] ERS-2 is a near-polar sun-synchronous orbit satellite with a mean local equator crossing time of 10:30 am. GOME, on board ERS-2, is a nadir-viewing spectrometer that measures radiances in four continuous bands (i.e., 237–315 nm, 312–406 nm, 397–609 nm, and 576–794 nm). Under normal operation, the GOME instrument, scans across track from east ($\sim -30^\circ$) to west ($\sim 30^\circ$) and back with a swath of 960 km, so that global coverage is achieved in three days in the equator. One nominal scan cycle of GOME lasts 6 s, 4.5 s for the forward scan and 1.5 s for the back scan; the forward scan consists of three pixels each with an area of $320 \times 40 \text{ km}^2$ and the back scan consists of one pixel with an area of $960 \times 40 \text{ km}^2$. Because of the large dynamical range of the signal in band 1, it is divided into two sub-bands (i.e., bands 1a and 1b) at 307 nm before 6 June 1998 and at 283 nm afterwards. The integration time for band 1a is 12 s, corresponding to 8 band-1b or band-2 pixels [ESA, 1995]. Because ozone profile retrievals use measurements in both bands 1 and 2, 8 pixels of measure-

ments in bands 1b and 2 are co-added to match the band 1a measurements. Therefore, the spatial resolution of our retrievals is normally $960 \times 80 \text{ km}^2$. In addition to radiance spectra, GOME measures direct solar irradiance via a Sun view mirror and diffuser plate on a daily basis [ESA, 1995]. The solar irradiance spectrum, measured on the same day, is used to normalize the measured earthshine radiance spectra.

[7] To validate the retrievals against TOMS, DB, and ozonesonde, we collocate GOME data with ozonesonde measurements ($\pm 1.5^\circ$ latitude and $\pm 12.5^\circ$ longitude) at 33 selected stations (see Table 1 and section 2.2) during 1996–1999. To validate against SAGE-II retrievals, we use the GOME data during 1996–1999. We use version 2.0 GOME Data Processor (GDP) extraction software [DLR, 2002], including all standard corrections (e.g., leakage current, stray light, polarization, degradation).

2.2. Other Data

[8] Ozonesonde data during 1996–1999 from 33 stations (Figure 1 and Table 1) are used to validate GOME TCO. For a global validation, we include stations from the far north (e.g., Resolute, 74.7°N) to the far south (e.g., Neumayer, 70.7°S) with at least one station in each 10° -latitude band between 80°N – 80°S . Data was primarily obtained from World Ozone and Ultraviolet Data Center (WOUDC, <http://www.woudc.org>). Some data unavailable or incomplete at WOUDC are directly obtained from the data originators (see Table 1). The measurements were made with three types of ozonesonde (Table 1). Ozonesonde techniques have different precisions, accuracies, and sources of errors. The Jülich Ozone Sonde Intercomparison Experiment (JOSIE) showed that measurements with different types of ozonesondes are typically within 10–20% with respect to the accurate UV photometer measurements and it was found that the precision of electrochemical concentration cell sondes is 5%, better than those of Brewer Mast and carbon iodine sondes (10–15%) [WMO, 1998]. The SHADOZ measurement precision is also estimated to be $\pm 5\%$ [Thompson *et al.*,

2003a]. Because each sonde launched is essentially a new instrument, it is difficult to evaluate the accuracy of ozone-sonde observations as a whole [Thompson *et al.*, 2003a].

[9] Nineteen of the 33 ozonesonde stations have DB TO measurements archived at WOUDC (Figure 1 and Table 1). The accuracy of well-calibrated DB measurements is estimated to be 3% or better [Basher, 1982; Kerr *et al.*, 1988; Kerr and McElroy, 1995]. For TOMS TO measurements, we use level-3 Earth-Probe (EP) TOMS data (<http://toms.gsfc.nasa.gov>), reprocessed with the recent TOMS Version-8 (V8) algorithm [Bhartia and Wellemeyer, 2002] and gridded in 1.25° longitude \times 1° latitude bins. Labow *et al.* [2004] validated TOMS V8 data against ground-based TO data and found the mean agreement is usually within 3%. For SAGE-II ozone profiles, we use the version 6.2 data above ~ 15 km during 1996–1999. Wang *et al.* [2002] assessed the quality of SAGE-II version 6.1 ozone data and found the mean agreement between SAGE-II and ozonesondes is within 10% down to 15 km. Version 6.2 data are similar to version 6.1 data with differences usually $<0.5\%$ (<http://www-sage2.larc.nasa.gov>).

3. Algorithm Description

3.1. Introduction to Inversion Technique

[10] We use the well-known OE technique to invert sun-normalized radiance spectra and derive ozone profiles. We review some of the basics here; readers are referred to Rodgers [2000] for more details. The idea of non-linear OE is to simultaneously and iteratively minimize the difference between measured and simulated radiances and the difference between retrieved (\mathbf{X}) and a priori (\mathbf{X}_a) state vectors, constrained with measurement error covariance matrix (\mathbf{S}_y) and the a priori covariance matrix (\mathbf{S}_a). The cost function χ^2 can be written:

$$\chi^2 = \left\| \mathbf{S}_y^{-\frac{1}{2}} \{ \mathbf{K}_i (\mathbf{X}_{i+1} - \mathbf{X}_i) - [\mathbf{Y} - \mathbf{R}(\mathbf{X}_i)] \} \right\|_2^2 + \left\| \mathbf{S}_a^{-\frac{1}{2}} (\mathbf{X}_{i+1} - \mathbf{X}_a) \right\|_2^2, \quad (1)$$

where \mathbf{X}_{i+1} and \mathbf{X}_i are the current and previous state vectors, respectively; \mathbf{Y} is the measurement vector; \mathbf{R} is the forward model and $\mathbf{R}(\mathbf{X}_i)$ are the simulated radiances with \mathbf{X}_i ; \mathbf{K}_i is the weighting function matrix, defined as $\partial \mathbf{R} / \partial \mathbf{X}_i$. \mathbf{S}_y is generally assumed diagonal without correlation between adjacent measurements. The a posteriori solution is given as:

$$\mathbf{X}_{i+1} = \mathbf{X}_i + \left(\mathbf{K}_i^T \mathbf{S}_y^{-1} \mathbf{K}_i + \mathbf{S}_a^{-1} \right)^{-1} \cdot \left\{ \mathbf{K}_i^T \mathbf{S}_y^{-1} [\mathbf{Y} - \mathbf{R}(\mathbf{X}_i)] - \mathbf{S}_a^{-1} (\mathbf{X}_i - \mathbf{X}_a) \right\}. \quad (2)$$

[11] The keys to retrievals are to accurately calibrate the measurements, to accurately simulate measurements, and to have good knowledge of measurement errors and the a priori covariance matrix.

3.2. Wavelength and Radiometric Calibrations

[12] Knowledge of instrumental line shape is important for convolving high-resolution spectroscopic cross sections to the GOME resolution and performing wavelength calibrations. Siddans [2003] found that errors in the slit

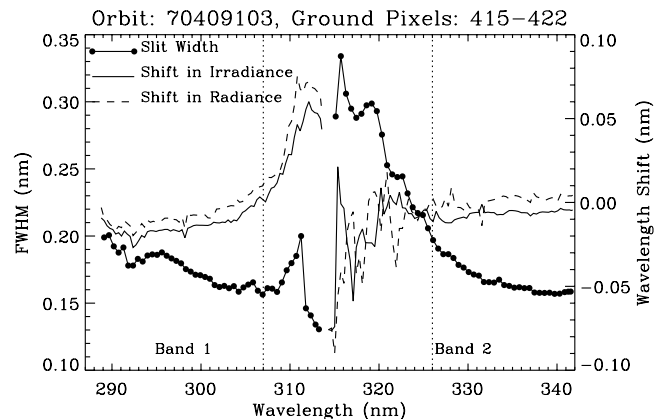


Figure 2. GOME slit width (line with circles, left axis), wavelength shifts in irradiances (solid line, right axis) and radiances (dashed line, right axis) versus wavelength in 280–340 nm for ground pixels of 415–422 in orbit 70904103 (center geo-location: 48.4°N , 7.8°E).

function can cause large errors in the retrieved tropospheric ozone. Chance [1998] found that using Gaussian slit functions can reduce fitting residuals than using GOME pre-flight slit measurements (parabolic), so we also assume Gaussian slit function. Using other slit functions (i.e., symmetric/asymmetric voigt, asymmetric Gaussian) does not improve the retrieval. The Gaussian slit width is determined using a non-linear least squares technique based on an well-calibrated (wavelength positions accurate to 0.002 nm and 0.0001 nm below and above 305 nm, respectively) high-resolution solar reference spectrum [Chance, 1998]. GOME slit widths vary substantially with wavelength, especially in the Huggins bands [Siddans, 2003; M. van Roozendaal, personal communication, 2003]. To account for variable slit widths in GOME measurements, we pre-fit the slit widths over a range of 21 spectral pixels in 5-pixel increments. Figure 2 (solid circles) shows an example of the derived slit widths in 288–342 nm. The slit widths show large variation at the end of band 1 (before ~ 312 nm) and at the beginning of band 2 (after ~ 312 nm). In our retrievals, we derive the slit widths for each solar irradiance spectrum and interpolate the slit widths for radiance/irradiance wavelength calibrations, the convolution of high resolution cross sections, and the undersampling correction.

[13] Before normalizing the radiances with irradiances, their wavelength positions need to be properly aligned; misalignment is due to the Doppler effect and other shifts (e.g., thermally-induced). Variable wavelength shifts for both radiances and irradiances relative to the accurately-calibrated solar reference spectrum are determined over a range of 15 spectral pixels in 3-pixel increments. Figure 2 also shows an example of the pre-fitted wavelength shifts for both solar irradiances (solid line) and radiances (dashed line) in 288–342 nm. Large shifts occur at the end of band 1 and at the beginning of band 2 and several large fluctuating structures occur between 314–325 nm. In the retrieval, we further fit the derived shifts with a 3rd-order polynomial. Using smoothed wavelength shifts improves the retrieval and reduces the fitting residual by $\sim 15\%$. The large

fluctuating structures, especially in the Huggins bands, may be caused by residual ozone absorption structures in the high-resolution reference spectrum, errors in the slit function, or the use of slit shape different from the assumed Gaussian shape. In addition to pre-calibrations before the retrievals, we fit the relative wavelength shifts between radiance and irradiance as part of the ozone profile retrieval with a 3rd-order polynomial. We also fit the shifts between all the trace gas cross section spectra and the measured radiance spectrum in the retrieval.

[14] According to the Nyquist criterion [Goldman, 1953], substantial spectral undersampling occurs in band 1 and in the spectral region of 325–342 nm (band 2) because the spectral sampling rate for GOME is ~ 0.11 nm/pixel while the spectral resolution is 0.10–0.20 nm (Figure 2). Chance [1998] developed an undersampling correction technique using the high-resolution solar reference spectrum to compensate for more than 90% of systematic fitting residuals in GOME BrO fitting. In our ozone profile retrieval, we perform a similar undersampling correction except that we use variable slit widths. With this correction, the fitting residual is reduced by $\sim 30\%$.

[15] GOME has degraded over time. Although a degradation correction is applied in the standard GDP extraction software, it is assumed that radiance and irradiance spectra degrade in the same way. *van der A et al.* [2002] found the solar radiances degrade differently from irradiances, especially in band 1 since 1998. Without degradation correction after 1998, the retrieval can be significantly affected or even cannot proceed [van der A et al., 2002; Latter et al., 2003]. After examining the derived wavelength-dependent degradation in the normalized radiances [van der A et al., 2002; Latter et al., 2003], we find the degradation mainly occurs in band 1 and the degradation curves can be approximated by polynomials. In our retrieval, a wavelength dependent correction (2nd-order polynomial) is simultaneously fitted to the normalized radiances only in band 1. The TO information from band 2, which is subject to less degradation, implicitly constrains the height-resolved information from band 1.

[16] Over South America and the South Atlantic ($\sim 0^\circ$ – 45° S, 0° – 75° W), GOME measurements are affected by the South Atlantic Anomaly (SAA); high-energy protons trapped inside the Earth's inner van Allen radiation belt impact the GOME detectors, leading to large data spikes especially in band 1 where the signal is low. The effect can be so severe that retrievals cannot proceed [Siddans, 2003]. Based on the fact that the ratio of radiances between adjacent pixels only slightly changes with ozone profile and band 2 measurements are less affected by SAA due to the stronger signal level, we assume the average of the first 10 band-2 pixels are correct. In the 2nd–4th iterations of the retrievals, we adjust the intensity of the longest band-1 pixel by matching the measured ratio of the average of the first 10 band-2 pixels to that pixel with the corresponding simulated ratio. Intensities of shorter band-1 spectral pixels are successively adjusted using the simulated ratios between adjacent pixels.

[17] Ozone absorption structures in band 1 are broad compared to those in the Huggins bands and the retrieval is not very sensitive to the spectral resolution of the measurements. Following the approach of Siddans [2003],

we co-add 5 adjacent spectral pixels with a step size of 2 spectral pixels for band-1 measurements. This co-adding not only significantly speeds up the retrieval but also reduces fitting residuals by 10–20%.

3.3. Forward Model and Its Inputs

[18] We use the Linearized Discrete Ordinate Radiative Transfer model (LIDORT) as the forward model to simulate radiances and weighting functions [Spurr et al., 2001]. The version of LIDORT used here implements the pseudo-spherical approximation [Spurr, 2002] for the direct-beam attenuation, which enables the backscattered radiances to be accurately obtained for a range of Solar Zenith Angles (SZAs) up to 90° within 0.3% in the nadir direction [Caudill et al., 1997; Spurr, 2002]. For the large GOME pixel used in the retrieval, the average view angle is $\sim 20^\circ$ and the error is $< 1\%$ for an SZA of 85° . The version of LIDORT used here is scalar (no polarization). The neglect of polarization can cause errors up to 10% in the backscattered radiances in a Rayleigh atmosphere [Mishchenko et al., 1994]. This error is corrected using a pre-calculated look-up table of scalar errors as functions of wavelength, TO, surface albedo and pressure, and viewing geometry (R. F. van Oss, personal communication, 2003). Six streams are used in the calculation. *van Oss and Spurr* [2002] found that radiances and weighting functions are normally accurate within 0.65% and 2%, respectively when using six streams.

[19] The Ring effect can be treated by convolving the Fraunhofer spectra and trace gas cross sections with rotational Raman cross sections [Chance and Spurr, 1997]. This approach may be inadequate to account for the dependence of Ring effect on factors such as the ozone profiles and the SZA because the optical thickness of the atmosphere due to ozone absorption changes by several orders of magnitude in the wavelength range used in retrievals. Instead, the Ring spectrum is obtained directly by modeling the first-order RRS of the direct beam [Sioris and Evans, 2000] for the same atmosphere used in the retrieval, accounting for the RRS dependence on viewing geometry, atmospheric ozone and temperature profiles. The Ring spectrum is only updated in the retrieval iteration when TO changes by ≥ 20 DU. Because multiple scattering is not considered in this Ring model, a scaling parameter is fitted in the retrieval for band 1; 2nd-order polynomial scaling parameters are fitted in band 2 to account for larger variation in multiple scattering effects. We use the actual GOME solar irradiances instead of the high-resolution reference spectrum because using the former reduces the fitting residuals by ~ 5 – 10% . This Ring model reduces the fitting residual by 15–25% compared to using the simple Fraunhofer approach.

[20] We treat clouds as Lambertian reflecting surfaces. Partial clouds are treated using the Independent Pixel Approximation (IPA) by assuming a cloud reflectivity of 80%. In the IPA, we need to know the cloud-top pressure and cloud fraction to model the clouds. We use the cloud-top pressure from the GOME Cloud Retrieval Algorithm (GOMECAT) [Kurosu et al., 1998]. The initial surface albedo is based on the GOME surface albedo database of *Koelemeijer et al.* [2003]; cloud fraction is then derived from measured GOME reflectance at 368–372 nm, where atmospheric absorption is minimal, and then is fixed in the

remaining steps. For full cloudy scenes, the cloud surface albedo is allowed to vary, but for partially cloudy scenes, the cloud reflectivity is taken to be fixed at 80%. In the retrieval, surface albedos are varied. A wavelength-independent surface albedo is used for band 1 and a wavelength-dependent surface albedo (i.e., 2nd-order polynomial) is used for band 2. To reduce aerosol effects on retrieval, we use monthly mean SAGE-II stratospheric background aerosols [Bauman *et al.*, 2003] and tropospheric aerosols based on monthly-mean mass fields from the Global Ozone Chemistry Aerosol Radiation and Transport (GOCART) model [Chin *et al.*, 2002] as described in Martin *et al.* [2003]. In addition, the wavelength-dependent surface albedo can account for some residual aerosol effects. We use daily surface pressure from National Centers for Environmental Prediction (NCEP) reanalysis data (<http://www.cdc.noaa.gov>) and daily European Center for Medium-Range Weather Forecasts (ECMWF) temperature profiles (<http://www.ecmwf.int>). Ozone is the only trace gas treated in the optical property input to LIDORT. We fit the cross sections of NO₂ [Yandaele *et al.*, 2003], SO₂ [Bogumil *et al.*, 2003], and BrO [Wilmouth *et al.*, 1999] to the normalized radiances with scaling and shift parameters.

[21] The quality of ozone and Rayleigh cross sections directly affects the retrieval accuracy. We use the ozone absorption cross sections by Brion *et al.* [1993] because they have more accurate wavelength calibration [Orphal, 2003] and the fitting residuals are reduced by 10–20% compared to using Bass-Paur (BP) cross sections [Bass and Paur, 1985] and GOME flight-model cross sections [Burrows *et al.*, 1999]. The Rayleigh cross sections are from Bodhaine *et al.* [1999] and are accurate to better than 0.002% over the range 250–550 nm. The depolarization factors accounting for molecular anisotropy are taken from Bates [1984].

[22] GOME provides viewing geometries at three points, the west edge, middle, and east edge of a ground pixel. We calculate the effective View Zenith Angle (VZA) and SZA by integrating and averaging the path lengths from west edge to east edge and calculate the effective Azimuth Angle (AZA) by averaging the AZAs at west and east edges. For the large pixels used for ozone profile retrieval, the effective VZA is usually $\sim 20^\circ$ and the AZA is near 90° .

[23] Weighting functions with respect to ozone profile elements and wavelength-independent albedo are directly calculated with LIDORT. Weighting functions for ozone cross section shift parameters and high-order albedo parameters are derived from those calculated weighting functions. For all the other auxiliary parameters, we calculate weighting functions with the finite difference approach.

3.4. Retrieval Scheme

[24] The fitting windows in our retrievals are 289–307 nm and 326–339 nm (Figure 2). Although measurements below 289 nm provide height-resolved information at high altitudes, we exclude them because of large measurements errors, NO γ band emission lines, and more severe instrument degradation [Hoogen *et al.*, 1999]. Including band-1b measurements in 307–314 nm and band-2 measurements in 313–326 nm should increase the tropospheric ozone information. However, we found that including those measurements lead to much worse comparisons with respect to

collocated ozonesonde TCO. The reasons for worse retrievals with more measurements are likely the large variation in wavelength shifts and slit widths for these measurements (Figure 2) and inconsistent intensity calibrations between these measurements and the ones used in the retrieval.

[25] Partial column ozone is retrieved on an 11-layer Umkehr or SBUV-like grid due to the limited vertical resolution from nadir-view observations. Each layer is approximately 5-km thick except for the top layer, which is ~ 10 -km thick. In addition, tropospheric layers are modified using tropopause and surface pressure so that tropopause is one of the retrieval levels. We use daily tropopause pressure from NCEP reanalysis data to separate the stratosphere from the troposphere. There are usually two or three layers in the troposphere. Tropospheric and stratospheric column ozone can be easily integrated from retrieved ozone profiles. In forward calculations, we can split each layer to a selected number of sub-layers and insert a layer for cloud top to improve the accuracy of forward modeling. Typically, we perform the radiative transfer calculation on a 23-layer atmosphere; using more layers only slightly changes the retrieved profiles, as shown in section 3.6.

[26] The measurement vector \mathbf{Y} in our algorithm is the logarithm of the corrected sun-normalized radiance spectra (ignoring wavelength calibrations):

$$\mathbf{Y} = \ln \left[\mathbf{I}_{\text{meas}} / \left(\mathbf{F}_{\text{meas}} \times a_{\text{deg},\text{total}} + \sum_{j=1}^2 a_{\text{us},j} \mathbf{F}_{\text{us},j} \right) \right], \quad (3)$$

where \mathbf{I}_{meas} is the extracted GOME radiance; \mathbf{F}_{meas} is the extracted GOME irradiance; $\mathbf{F}_{\text{us},j}$ are the undersampling correction spectra and $\alpha_{\text{us},j}$ are the corresponding scaling parameters; $\alpha_{\text{deg},\text{total}}$ is the degradation polynomial. The simulated normalized radiance \mathbf{R} is the LIDORT-calculated radiance ($\mathbf{R}_{\text{LIDORT}}$) with additional correction:

$$\mathbf{R} = (\mathbf{R}_{\text{LIDORT}} + \mathbf{R}_{\text{polcorr}}) \exp \left(- \sum_{j=0}^2 a_{\text{ring},j} \phi_{\text{ring}} - \sum a_{\text{tr},j} \phi_{\text{tr},j} \right), \quad (4)$$

where $\mathbf{R}_{\text{polcorr}}$ is the correction in radiance due to neglecting polarization; ϕ_{ring} is the Ring spectrum and $\alpha_{\text{ring},j}$ are the corresponding Ring scaling parameters; $\phi_{\text{tr},j}$ are the cross sections for minor trace gases and $\alpha_{\text{tr},j}$ are the corresponding scaling parameters. The state vector consists of 47 parameters including 11 elements for the 11 layers of column ozone. It also includes one albedo parameter for band 1, three albedo parameters for band 2, four cross section shift parameters for each band, four radiance/irradiance wavelength shift parameters for each band, one scaling and wavelength shift parameters for each minor species, two parameters for undersampling correction, one Ring scaling parameter for band 1 and three parameters for band 2, three degradation correction parameters in band 1, and one parameter to account for residual dark current.

[27] We use the estimated random-noise errors provided in GOME data as measurement errors. The a priori information is from the TOMS V8 climatology [McPeters *et al.*,

2003]. This climatology, derived from 15 years of SAGE, Microwave Limb Sounder (MLS), and ozonesonde observations, provides ozone-mixing ratios and their Standard Deviations (SDs) at 61 levels from 0 to 60 km for each month and each 10°-latitude band. A correlation length of six km is used in the construction of the a priori covariance matrix. The a priori error for zero-order albedo is assumed to be 0.04. A priori errors for other parameters are assumed to be five times of the average retrieved values; they are assumed uncorrelated with each other and also uncorrelated with any of the ozone profile elements.

[28] Retrievals are defined to converge when the change in retrieved ozone at each layer is less than 1% or the relative change in χ^2 is less than 1%. When an orbit of data is processed at a time and the retrieval of one pixel is used as the initial guess of the next pixel, most retrievals converge in 2–3 iterations. It takes about ~ 70 minutes to process one orbit of GOME data on a 2.0-GHz processor. This algorithm would be able to process the GOME (or GOME-2) data operationally with modest computer resources. With all of the above calibrations and improvements in radiative transfer simulations, the average Root-Mean-Square (RMS) of the fitting residuals is reduced to $\sim 0.30\%$. For the Huggins bands, the average RMS is reduced to $\sim 0.17\%$.

[29] In our algorithm, the ghost column (i.e., column ozone below clouds) is implicitly handled through the ozone weighting functions and smoothing from above clouds. Under overcast conditions, weighting functions for ozone below cloud are zero, so ozone below clouds in the retrieved ozone profile is updated through only smoothing. If the scene is partially cloudy, weighting functions for ozone below clouds are those for the clear-sky part multiplied by clear-sky fraction, and ozone below clouds is updated according to the weighting functions as well as smoothing as the retrieval process proceeds.

3.5. Retrieval Characterization

[30] The Averaging Kernels (AKs), defined as the sensitivity of the retrieved state $\hat{\mathbf{X}}$ to the true state \mathbf{X} , contain very useful information to characterize the retrieval [Rodgers, 2000]:

$$\mathbf{A} = \frac{\partial \hat{\mathbf{X}}}{\partial \mathbf{X}} = \left(\mathbf{K}^T \mathbf{S}_y^{-1} \mathbf{K} + \mathbf{S}_a^{-1} \right)^{-1} \mathbf{K}^T \mathbf{S}_y^{-1} \mathbf{K} = \hat{\mathbf{S}} \mathbf{K}^T \mathbf{S}_y^{-1} \mathbf{K}, \quad (5)$$

where $\hat{\mathbf{S}}$ is the solution error covariance matrix. Other useful characterization tools can be derived from AKs. The sum of diagonal elements of the AK matrix is called the “Degrees of Freedom for Signal (DFS)”, which describes the number of independent pieces of information available from measurements; each diagonal element indicates the DFS at an individual retrieval layer. The Full Width at Half Maximum (FWHM) of averaging kernels generally indicates the Vertical Resolution (VR). A row of AKs at a given layer indicates the sensitivity of retrieved ozone at that layer to changes in ozone at all the layers. Because only the differences between true and a priori values contribute to the retrieval at a certain layer, we need to weight the contributions from all the layers by those differences, which can be represented by the a priori SD. Then the a priori influence $f_{a,i}$ at a layer i can be defined as one minus the

contributions from all the layers weighted by a priori SD $\varepsilon_{a,i}$ at all the layers:

$$f_{a,i} = 1 - \sum_{j=1}^n (\mathbf{A}_{ij} \varepsilon_{a,j} / \varepsilon_{a,i}), \quad (6)$$

where n is the number of retrieval layers. An $f_{a,i}$ value close to 0 (1) indicates that the retrieval information at that layer mainly comes from the measurements (the a priori), respectively. The retrieval efficiency $\eta_{r,i}$, a measure of the retrievable fraction of the partial column ozone in layer i that deviates from the a priori [Hudson *et al.*, 1995] can be derived as follows:

$$\eta_{r,i} = \sum_{j=1}^n \mathbf{A}_{ji}, \quad (7)$$

because a column of AKs at a given layer gives the column ozone response in all layers to a unit perturbation at that layer. We propose similar concepts to characterize the retrieved TCO. The tropospheric DFS is the sum of DFS at all tropospheric layers. Since we know from equation (6) the a priori influence for each tropospheric layer, the a priori influence in the retrieved TCO (f_{ta}) can be derived by averaging $f_{a,i}$ in tropospheric layers weighted by their ozone variability:

$$f_{ta} = \sum_{i=1}^{n_t} f_{a,i} \varepsilon_{a,i} / \sum_{i=1}^{n_t} \varepsilon_{a,i}, \quad (8)$$

where n_t is the number of tropospheric layers. In this defined f_{ta} , the smoothing from the stratosphere to the troposphere is not considered as a priori influence. To quantify the contribution that does not come from actual tropospheric ozone (f_{tat}), $f_{a,i}$ in equation (8) can be replaced by the a priori influence in the troposphere ($f_{at,i}$), which can be derived from (6), except replacing n with n_t . The retrieval efficiency for TCO (η_{tr}) can be derived as:

$$\eta_{tr} = \sum_{i=1}^{n_t} \eta_{r,i} \varepsilon_{a,i} / \sum_{i=1}^{n_t} \varepsilon_{a,i}. \quad (9)$$

Similarly, η_{tr} in equation (9) gives the fraction of TCO that can be retrieved in the TO instead of TCO. To describe the fraction of the true TCO actually retrieved as TCO (η_{trt}), $\eta_{r,i}$ in equation (9) can be replaced by the retrieval efficiency in TCO ($\eta_{rt,i}$), which can in turn be derived from (7) except replacing n with n_t . After transformation, f_{tat} and η_{trt} are actually complementary, i.e., $f_{tat} = 1 - \eta_{trt}$. The major assumption in the above derivation is that the climatological mean and SD reflect the true statistics.

[31] Figure 3 shows three examples of retrieval AKs under nearly clear conditions, representing high-latitude, midlatitude, and low-latitude conditions, respectively. For all the cases, the AKs for the top few layers show broad peaks and the peaks are dislocated downward. This occurs because we do not use measurements below 289 nm, which would provide more height-resolved information at those altitudes. For the high-latitude case (Figure 3a), the vertical distribution of ozone is best resolved over the altitude range

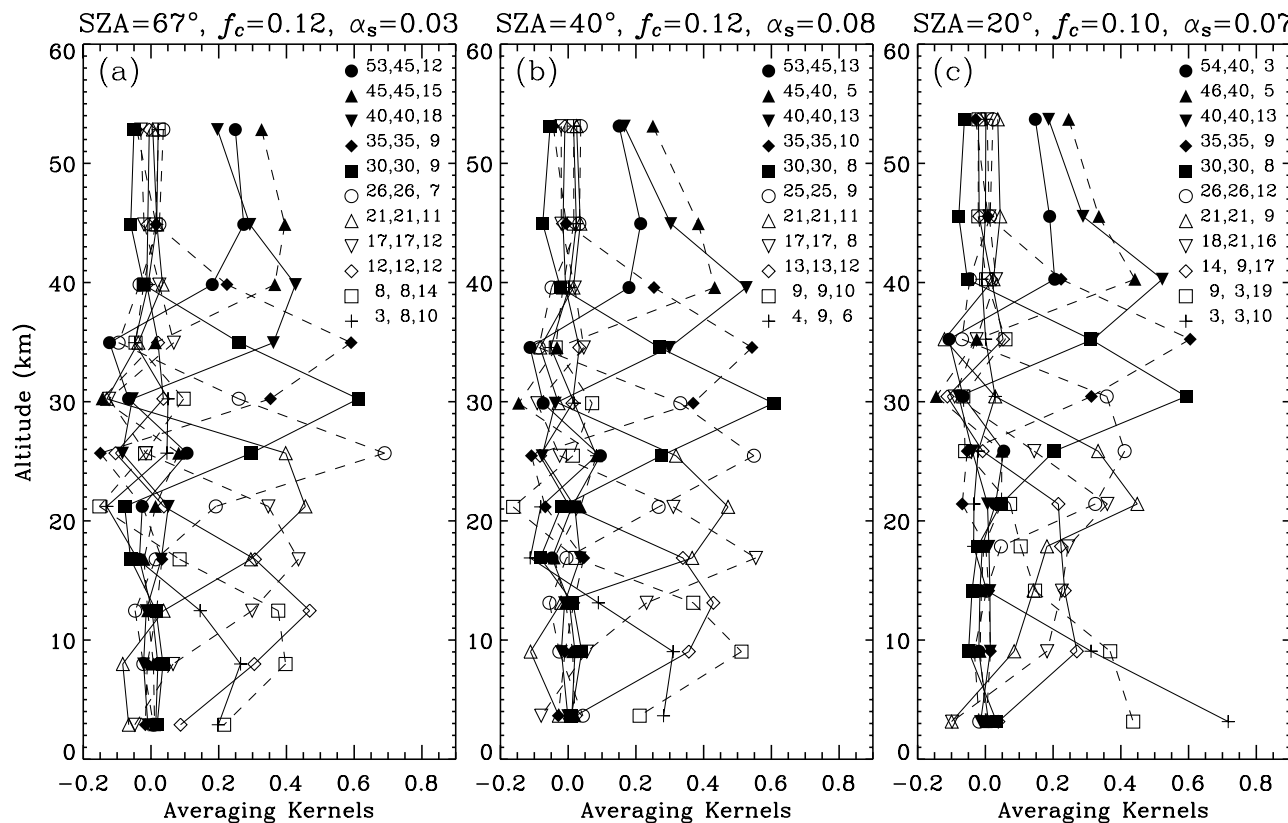


Figure 3. Three examples of retrieval Averaging Kernels (AKs) for (a) pixels 982–989 in orbit 60925092 near Sodankylä (66.6°N, 29.8°E), (b) pixels 728–735 in orbit 70409095 near Hohenpeißenberg (46.8°N, 15.0°E), and (c) pixels 887–895 in orbit 71010105 near Ascension Island (9.0°S, 12.8°W). The solar zenith angle (SZA), cloud fraction (f_c), and surface albedo (α_s) are shown on the titles. The numbers following the symbols show the nominal altitude (km) of AKs, the peak altitude (km) of AKs, and vertical resolution (km) in terms of full width at half maximum.

of ~ 10 – 37 km; the peak altitudes of AKs agree well with the nominal altitudes and the VRs are within 7–12 km. Because of limited photon penetration in the lower troposphere at larger SZAs, the peak altitudes near the surface are displaced upward and the retrievals are more sensitive to ozone at higher altitudes. The AKs for the midlatitude case (Figure 3b) are similar except that the altitude range that is well resolved extends downward to ~ 7 km because of increased photon penetration. For the tropical case (Figure 3c), the ozone profile is best resolved over 20–38 km with VRs of 8–12 km. There is much stronger sensitivity to ozone near the surface and the peak altitude of the bottom layer is not dislocated. However, we can see the VRs are poor over 6–20 km and the peak altitudes are dislocated upward for layer 4 and downward for layers 2 and 3. This is partly because we do not use measurements in the range of 307–325 nm, which would provide more height-resolved information for those altitude ranges under high-sun conditions.

[32] Table 2 summarizes the average retrieval characterizations at each layer for three latitude bands: tropics, midlatitudes, and high latitudes. The DFS of the top five layers are similar for these latitude bands. The DFS usually increase with latitude over ~ 10 – 20 km but decrease with latitude near the surface. The a priori influence $f_{a,i}$ is usually close to 0 except for the top and bottom layers; the retrieved

ozone near the surface is subject more to a priori influence at higher latitudes. The $\eta_{r,i}$ in TO is about 1 over ~ 10 – 60 km, so ozone at this altitude range is well retrieved in the TO. At layers 2 and 3 in the tropics and layer 2 in the midlatitudes, the $\eta_{r,i}$ is slightly larger than 1 because $\eta_{r,i}$ increases above clouds [Hudson *et al.*, 1995]. The peak altitudes of AKs are displaced downward for the top two layers. There are also significant displacements (i.e., >2 km) over 5–20 km in the tropics and over 0–10 km at higher latitudes. The VRs are usually within 7–14 km for altitudes with small vertical displacements (i.e., 20–45 km in the tropics, 5–45 km in the midlatitudes, and 10–50 km in the high latitudes).

[33] Figure 4 shows the average DFS in TO, Stratospheric Column Ozone (SCO), and TCO for all the ozonesonde stations used as a function of latitude. Both total (4.5–5.5) and stratospheric (3.5–4.5) DFS increase with latitudes. The tropospheric DFS vary from ~ 0.5 at higher latitudes to ~ 1.2 in the tropics. Figure 4 also shows the f_{ta} , η_{tr} , and f_{iat} (i.e., $1 - \eta_{tr}$) as a function of latitude. The average f_{ta} increases with latitude and is usually $<30\%$. The a priori influence that does not come from the troposphere (f_{iat}) is smaller than f_{ta} and shows large latitudinal variation, from $\sim 15\%$ in the tropics to $\sim 50\%$ at high latitudes. η_{tr} is close to 1 in the tropics and decreases to ~ 0.9 at higher latitudes. All the above parameters show

Table 2. Characterizations of Retrievals at Each Layer Averaged for Tropical, Midlatitude, and High-Latitude Stations^a

Layer	~Alt., km	Tropics (30°S–30°N)					Midlatitude (30°S/N–60°S/N)					High Latitude (60°S/N–80°S/N)				
		DFS	f_a	η_r	r	Δd	DFS	f_a	η_r	r	Δd	DFS	f_a	η_r	r	Δd
11	55.0	0.2	0.6	1.0	11.9	-8.4	0.2	0.4	1.2	9.5	-8.5	0.2	0.4	1.0	14.5	-7.1
10	47.5	0.4	0.0	1.0	6.3	-4.6	0.4	0.0	1.1	9.4	-2.4	0.4	0.0	1.1	12.6	-1.9
9	42.5	0.5	-0.2	1.0	13.8	0.0	0.5	-0.2	1.0	13.7	0.0	0.5	-0.2	1.0	14.2	0.1
8	37.5	0.6	0.0	1.0	8.8	0.0	0.6	0.0	1.0	10.1	0.0	0.6	0.0	1.0	10.2	0.1
7	32.5	0.6	0.1	1.0	8.6	0.0	0.6	0.0	1.0	8.1	0.0	0.6	0.1	1.0	8.5	0.1
6	27.5	0.4	0.0	1.0	12.0	1.0	0.5	0.0	1.0	9.7	0.0	0.7	0.0	1.0	7.3	0.1
5	22.5	0.5	-0.1	1.0	9.2	0.0	0.5	0.0	1.0	11.1	0.3	0.6	0.0	1.0	8.9	0.0
4	17.5	0.3	0.0	1.0	13.0	2.4	0.5	0.0	1.0	10.2	-0.1	0.5	0.0	1.0	10.1	0.7
3	12.5	0.3	0.0	1.1	16.0	1.0	0.5	-0.1	1.0	11.0	0.1	0.5	-0.1	1.0	9.3	0.9
2	7.5	0.4	0.0	1.2	15.8	-4.1	0.4	0.1	1.1	10.4	1.3	0.3	0.1	1.0	9.6	2.3
1	2.5	0.5	0.2	0.8	12.8	0.4	0.3	0.5	0.6	9.9	4.0	0.2	0.5	0.7	9.7	4.7

^aDFS, degrees of freedom for signal; f_a , a priori fraction; η_r , retrieval efficiency in total ozone; r , vertical resolution (km) in full width at half maximum; Δd , vertical displacement (km) of the peak of averaging kernels.

higher variability at higher latitudes primarily following the SZA variation.

3.6. Error Analysis

[34] According to Rodgers [2000], errors in the retrievals result from four sources: measurement errors, smoothing errors due to the limited VR of the retrieval, forward model parameter errors, and forward model errors. Measurement errors include both random noise errors and systematic measurement errors. Of these errors, the retrieval noise error ϵ_r (i.e., precision) and smoothing error ϵ_s are directly estimated in the retrieval according to the formulation in Rodgers [2000]. The Root Sum Square (RSS) of ϵ_r and ϵ_s is the solution error $\hat{\epsilon}$ (i.e., the square root of diagonal elements \hat{S} in equation (5)).

[35] Figures 5a, 5c, and 5e show the mean absolute ϵ_r , ϵ_s , $\hat{\epsilon}$, and ϵ_a (a priori standard deviation) for the tropics, midlatitudes, and high latitudes, respectively. The absolute retrieval errors are smallest in the tropics. In most cases, the

smoothing error component is the largest contribution to the solution error. The precisions are usually <2 DU and the solution errors are usually <5 DU. Figures 5b, 5d, and 5f show corresponding relative retrieval errors. The relative errors have similar magnitudes at different latitudes. The precisions are 2–8% in the stratosphere and are within 12% in the troposphere. The solution errors are usually within 10% between 20–40 km and increase to $\sim 15\%$ at higher altitudes and to $\sim 30\%$ at lower altitudes. The solution errors are much smaller than the a priori errors except for the top and bottom layers.

[36] The errors in the TO, SCO, and TCO can be derived from error covariance matrices by adding the errors at each layer and removing correlated errors within the

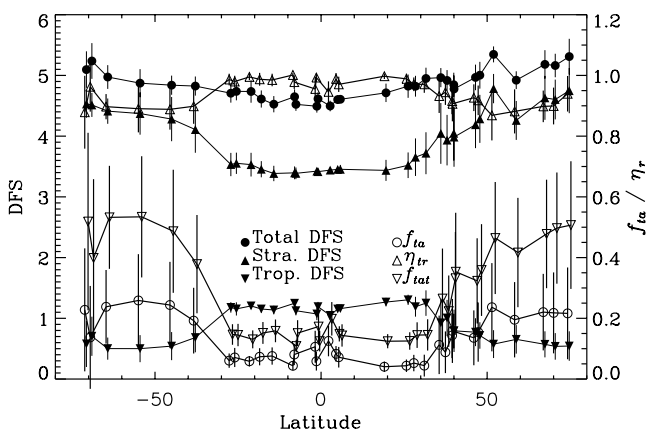


Figure 4. Mean and 1σ of Degrees of Freedom for Signal (DFS) in the whole atmosphere, stratosphere, and troposphere, tropospheric a priori fraction not from the measurements (f_{ia}), tropospheric retrieval efficiency in total ozone (η_{tr}), and tropospheric a priori fraction not from the troposphere (f_{iat}) for all the retrievals at each ozonesonde station. The axis is on the left for DFS and on the right for the others. For clarity, f_{ia} and η_{tr} are shifted to the left by 0.5° in latitude and f_{iat} is shifted to the right by 0.5° in latitude.

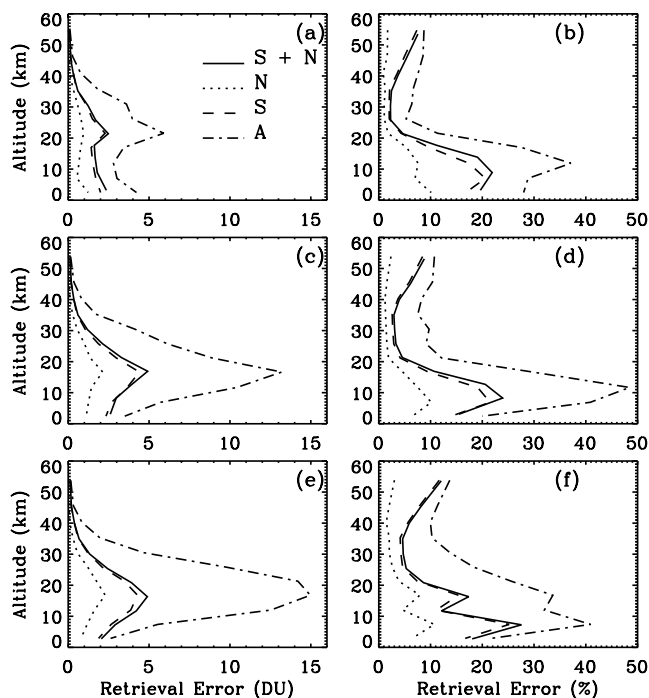


Figure 5. (a) Mean absolute solution errors (S+N), smoothing errors (S), retrieval noise errors (N), and a priori errors (A) in the tropics (30°S–30°N). (b) Same as Figure 5a, but for relative retrieval errors. (c)–(d) and (e)–(f) Same as Figures 5a and 5b, but for midlatitudes (30°S/N–60°S/N) and high latitudes (60°S/N–80°S/N), respectively.

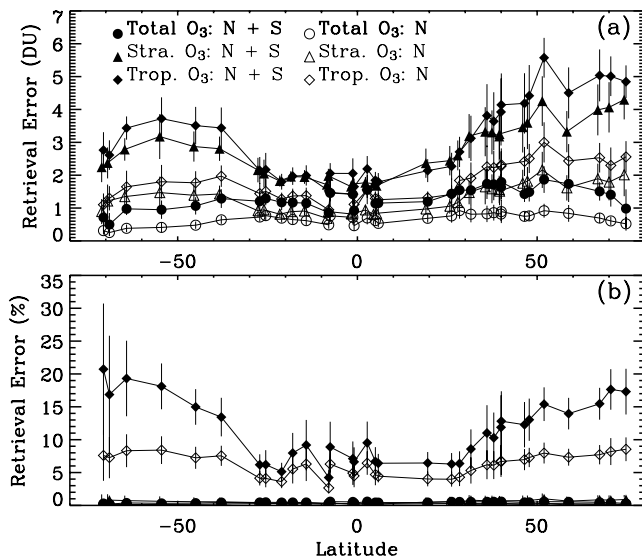


Figure 6. (a) Mean and 1σ of the absolute solution errors (S+N) and retrieval noise errors (N) in total, stratospheric, and tropospheric column ozone at all the stations. (b) Same as Figure 6a, but for relative retrieval errors.

corresponding altitude ranges. Figure 6 shows both absolute (Figure 6a) and relative (Figure 6b) ϵ_r and $\hat{\epsilon}$ and the 1σ at all the stations as a function of latitude. The precisions and solution errors in TO are usually within 2 DU (0.5%) and 3 DU (1.0%), respectively. For SCO, the precisions are generally within 2 DU (1%) and the solution errors usually range from 2 DU (1%) in the tropics to 5 DU (2%) at high latitudes. The errors in TCO are larger than those of TO and SCO. The precisions in TCO are usually within 1.5 DU (6%) in the tropics and within 3 DU (12%) at higher latitudes. The solution errors are usually within 3 DU (12%) in the tropics and within 6 DU (25%) at higher latitudes.

[37] To estimate forward model errors, forward model parameter errors, and systematic measurement errors, we perform sensitivity tests for 10 representative scenarios (Table 3). These scenarios are selected from actual GOME data so that we can perform error assessment using the retrieval algorithm. For each source of error, we perform retrievals with the perturbed measurements or forward model parameters or by changing model options. The differences between these perturbed retrievals and the standard retrievals isolate the retrieval errors due to an individual source. We then get the RMS errors of these 10

scenarios. Table 4 summarizes the mean retrieval errors at each layer and also in TO, TCO, and SCO from different sources along with the precisions, smoothing errors, solution errors, and a priori errors.

[38] In addition to the random-noise measurement errors considered in the retrievals, we examine four measurement errors (Table 4). GOME is a polarization sensitive instrument and the radiometric calibration requires the polarization of the incoming light. However, the standard polarization correction in GDP v2.0 using measured broadband polarization introduces radiance errors of up to 10% [Schutgens and Stammes, 2003]. Schutgens and Stammes [2003] developed an improved polarization correction to reduce the radiance errors to $<3\%$ in the UV. This algorithm is implemented in the GOMECAL software (http://www.knmi.nl/gome_fd/gomecal). We compare the retrievals with and without this improved polarization correction to represent the retrieval errors due to inadequate instrumental polarization correction. From Table 4, the retrieval errors due to these error sources are insignificant compared to the smoothing errors and precision, $<5\%$ for individual layers, $<2.5\%$ for TCO, and $\leq 0.3\%$ for SCO and TO.

[39] We assess six systematic forward model errors (Table 4). The corresponding retrieval errors are also insignificant relative to precision and smoothing errors, $<5\%$ for individual layers, $<4\%$ for TCO, and $\leq 0.4\%$ for TO and SCO. van Oss *et al.* [2001] found the scalar approximation can introduce retrieval errors of 10–18% in the troposphere, but these errors are reduced to $<3\%$ at all layers after the radiance polarization correction. The much smaller improvement in our algorithm is probably because we do not use the measurements between 307 and 325 nm where radiance errors due to the scalar approximation show large variation, and our algorithm can partly correct the broadly-structured part of the radiance errors through the wavelength-dependent albedo.

[40] We examine 12 forward model parameter errors (3 random and 9 systematic, Table 4). The most significant random error is the precision in ozone cross section; an error of only 0.2% random error leads to $\sim 6\%$ retrieval errors for individual tropospheric layers, 5% for TCO, and 0.6% for SCO. The significant sources of systematic errors for tropospheric ozone are the 20-mb error in tropopause pressure, the 3 K temperature error at all layers, and the 100-mb error in cloud-top pressure. They lead to 5–8% errors in TO and 3–11% at individual tropospheric layers. For TO and SCO, the significant sources of systematic errors are the 1% error in ozone cross section, the 20-mb error in tropopause (only for SCO), the 100-mb error in

Table 3. Ten Representative Cases Used in Sensitivity Analysis: Tropical, Midlatitude Summer and Winter, High-Latitude Summer and Winter for Both Nearly Clear and Overcast Conditions^a

Latitude Bands	Clear							Cloudy						
	θ_0	α_s	τ_t	ω_a	τ_s	f_c	p_c	θ_0	α_s	τ_t	ω_a	τ_s	f_c	p_c
Tropics	24.3	0.06	0.04	0.84	0.005	0.05	277	24.4	0.05	0.15	0.83	0.006	0.82	488
Midlatitudes	27.6	0.05	0.51	0.86	0.007	0.05	754	26.6	0.05	0.45	0.86	0.008	0.78	550
	70.0	0.05	0.31	0.84	0.01	0.07	721	70.2	0.09	0.27	0.83	0.01	0.82	682
High latitudes	45.1	0.09	0.32	0.88	0.008	0.0		47.0	0.09	0.28	0.90	0.008	0.78	676
	80.2	0.94	0.14	0.92	0.01	0.0		76.0	0.27	0.18	0.93	0.008	0.86	687

^aThe solar zenith angle (θ_0), surface albedo (α_s), aerosol optical thickness at 340 nm (τ_t) and average aerosol single scattering albedo (ω_a) in the troposphere, aerosol optical thickness in the stratosphere (τ_s), cloud fraction (f_c), and cloud-top pressure (p_c , hPa) are shown for each case.

Table 4. Summary of the Relative (%) Measurements Errors, Forward Model Errors, and Forward Model Parameter Errors at Each Layer and in the Tropospheric, Stratospheric, and Total Column Ozone (TCO, SCO, and TO), Along With the Precisions, Smoothing Errors, Solution Errors, and a Priori Errors^a

Source of Errors	Layers (From Surface to Top of the Atmosphere)											Column Ozone		
	1	2	3	4	5	6	7	8	9	10	11	TCO	SCO	TO
	<i>Measurement Errors (S, Systematic; R, Random)</i>													
1% error in radiance (S)	1.3	2.5	0.9	0.4	0.2	0.3	0.2	0.4	0.5	0.5	0.0	1.9	0.1	0.1
0.1 nm error in wavelength (S)	0.0	0.1	0.1	0.0	0.0	0.0	0.0	0.0	0.0	0.0	0.0	0.0	0.0	0.0
0.002 nm error in wavelength (R)	2.4	3.2	4.0	1.2	1.8	0.6	0.8	1.8	2.0	1.0	0.4	2.4	0.2	0.2
Instrumental polarization corr. (S)	1.3	4.5	4.7	3.7	2.1	3.8	1.8	2.5	2.1	2.1	0.4	2.9	0.3	0.2
	<i>Forward Model Errors (Systematic)</i>													
6 stream versus 20 stream	2.1	4.3	4.8	1.2	1.7	1.5	0.9	1.2	1.7	1.3	0.2	3.9	0.4	0.4
22 layers versus 66 layers	1.7	3.5	3.7	1.1	1.0	1.0	1.0	1.1	1.4	1.2	0.3	2.5	0.3	0.1
50 mb offset in tropopause ^b														0.1
1 versus 3 view geometry	0.5	0.8	0.6	0.4	0.1	0.1	0.1	0.1	0.1	0.1	0.0	0.6	0.0	0.1
Radiance polarization correction	1.9	4.1	3.0	0.9	0.5	0.9	1.0	1.8	2.0	1.2	0.3	2.9	0.3	0.3
	<i>Random Forward Model Parameter Errors</i>													
0.2% O ₃ Cross Section (CS) error	4.3	5.9	5.9	0.9	2.0	1.0	1.2	1.8	1.8	2.0	2.1	5.0	0.6	0.2
0.05% Rayleigh CS error	0.2	0.7	0.7	0.2	0.2	0.1	0.1	0.1	0.1	0.1	0.1	0.7	0.0	0.0
0.002 nm error in O ₃ wavelength	0.2	0.7	0.1	0.2	0.0	0.1	0.3	0.3	0.3	0.3	0.1	0.5	0.1	0.0
	<i>Systematic Forward Model Parameter Errors</i>													
1% error in O ₃ CS	0.3	0.8	1.4	1.1	0.9	1.0	0.9	0.7	0.6	0.5	0.0	0.7	1.0	0.9
1% error in Rayleigh CS	0.4	0.9	0.8	0.6	0.3	0.3	0.6	0.7	0.8	0.5	0.4	0.6	0.1	0.1
0.01 nm in O ₃ wavelength	0.9	1.2	0.8	0.8	0.2	0.3	0.2	0.2	0.2	0.2	0.3	0.9	0.1	0.0
50% error initial surface albedo	0.7	1.7	1.4	0.3	0.5	0.4	0.2	0.3	0.2	0.1	0.0	0.9	0.1	0.2
20 mb error in surface pressure	2.0	1.5	0.7	0.1	0.1	0.1	0.9	0.9	0.6	0.3	0.2	1.6	0.1	0.1
100-mb error in cloud top pressure	6.0	7.1	3.4	1.3	1.1	0.4	0.6	1.0	0.8	0.5	0.3	5.4	0.5	0.9
Aerosols versus no aerosols	4.3	3.5	3.2	1.3	1.4	1.6	1.8	1.7	1.4	0.8	0.2	3.0	0.3	0.4
3 K temperature error at all layers	5.2	10.8	10.2	6.9	3.1	2.1	2.2	2.4	2.5	2.6	1.6	7.3	0.9	0.4
20 mb error in tropopause ^c												8.2	1.0	
Sum of above errors^d	11.1	17.1	15.6	8.5	5.4	5.3	4.2	5.2	5.2	4.6	2.8	15.1	2.0	1.5
Precisions	7.5	9.7	6.9	4.3	2.2	1.9	1.5	1.4	1.5	1.9	3.3	7.3	0.6	0.3
Smoothing errors	16.0	19.8	17.6	8.8	4.3	3.4	2.8	2.8	3.9	7.3	8.9	12.0	1.0	0.5
Solution errors	17.6	22.1	18.9	9.8	4.9	3.9	3.2	3.1	4.2	7.5	9.5	14.0	1.2	0.6
Total errors	20.8	28.9	24.5	13.0	7.3	6.5	5.3	6.1	6.6	8.8	9.9	20.6	2.3	1.6
A priori errors	22.7	40.4	49.2	25.9	15.8	14.6	13.1	10.4	11.1	13.8	14.3			

^aThese errors are RMS-averaged over the ten scenarios listed in Table 3.

^bThe errors are estimated by comparing the differences between the base case and the case with the tropopause pressure increased by 50 hPa. Because of the retrieval grid change, errors are reported only for TO.

^cThe errors are estimated by comparing the differences in TCO and SCO between ± 10 hPa tropopause pressure from the base case.

^dThe sum does not include the error due to radiance polarization correction since it is included in the algorithm.

cloud-top pressure, and the 3-K error in temperature, which introduce up to $\sim 1\%$ retrieval errors. *van Oss et al.* [2001] analyzed the errors due to aerosols and found 20% uncertainty in aerosol optical thickness introduces $\sim 3\%$ error in tropospheric ozone, larger than those we estimated if scaled to 100% uncertainty. This is mainly because we use a wavelength dependent albedo, which partly takes the effect of aerosols into account. We compare the retrieved TCO without and with aerosols as a function of tropospheric aerosol optical depth τ (0.05–0.95) and single scattering albedo ω (0.75–0.90) at 340 nm for one orbit of GOME data. The differences are within 4 DU and the mean difference is -0.14 ± 1.1 (1σ) DU; it does not show much dependence on ω and only shows slight dependence on τ . The effects on TO are similar and the mean difference is -0.38 ± 0.96 DU. Thus the aerosol effect in our algorithm is much smaller than that in the TOMS version 7 TO algorithm, in which errors of up to 10% in TO occur under high loading of UV-absorbing aerosols [Torres and Bhartia, 1999].

[41] The RSS of the above errors are much larger than the precisions, but smaller than smoothing errors in the troposphere (Table 4). The accuracy, defined as the RSS of all the

errors including smoothing and random-noise errors, is 20–30% in the bottom three layers and 5–13% for upper layers. The errors in TCO, SCO, and TO are $\sim 21\%$, 2.3%, and 1.6%, respectively. Compared to the a priori errors, the total errors are significantly reduced between layers 2 and 10. Note the above error assessment should be considered as a subset of sensitivity studies rather than a complete accuracy assessment because some errors are rather difficult to estimate (e.g., errors due to the assumption of homogeneous Lambertian clouds and the assumption of a homogeneous atmosphere and surface for a 960×80 km² area). We compare with correlative measurements in section 5 to better assess the accuracy of our retrievals.

4. Examples of GOME Retrievals

[42] Figure 7 shows an example of retrieved profiles of partial column ozone for the orbit 71022024 on 22 October 1997. Partial column ozone peaks at ~ 24 km in the tropics and at 16–22 km at higher latitudes, generally following the change in tropopause height. Inside the polar vortex region (80° – 70° S), we can see substantial thinning of stratospheric ozone layer due to chemical depletion at altitude range 16–

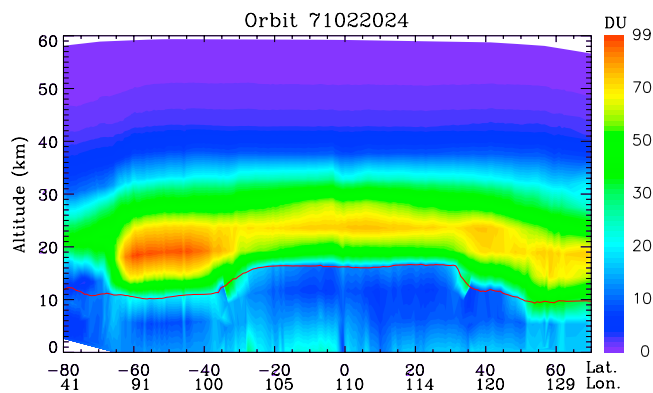


Figure 7. Retrieved profiles of partial (layer) column ozone (DU) for orbit 71022024 on 22 October 1997. The red line indicates the tropopause height.

35 km, with the smallest TO ~ 120 DU. Outside the polar vortex region (40° – 60° S), partial column ozone of 90–100 DU occurs at ~ 20 km layer with TO values of ~ 350 DU. Between 60° – 70° S, the stratospheric ozone layer gradually becomes thinner and the TO smoothly decreases from 350 DU to 150 DU. There is enhanced tropospheric ozone near the surface over the Southern India Ocean (25° – 30° S, 102° – 104° E) with TCO values of 45–60 DU, and over Indonesia (5° – 15° S, 106 – 109° E) with TCO values of 42–50 DU. The high amount of tropospheric ozone over the Southern India Ocean is due to the strong biomass burning activities during August–October in the southern hemisphere. The enhanced ozone over Indonesia is due to the 1997–1998 El Niño event, which led to intense biomass burning and changed meteorological conditions [Thompson *et al.*, 2001; Chandra *et al.*, 2002]. Between 25° S– 50° N, the ozone in the middle and upper troposphere is relatively low compared to that in the lower troposphere.

[43] Figure 1 shows a three-day composite global map of TCO on 22–24 October 1997 (global coverage in three days near the equator). High amounts of TCO (~ 40 – 60 DU) occur at southern midlatitudes (35° – 20° S), over the South Atlantic Ocean and South America (40° S– 0° S), consistent with the results of Chandra *et al.* [2003] and ozonesonde observations at Easter Island, Irene, and La Réunion during this month (results not shown). There are also enhanced TCO amounts of ~ 40 – 50 DU over Indonesia due to the 1997–1998 El Niño event [Thompson *et al.*, 2001; Chandra *et al.*, 2002]. High TCO values of ~ 30 – 45 DU also occur at northern midlatitudes (25° N– 40° N) and high latitudes. Low TCO values of < 21 DU occur over the tropical central and eastern Pacific (5° S– 20° N) and at the southern high latitudes (85° – 50° S). The validation of TCO spatial morphology is beyond the scope of this paper and will be presented in a following paper by comparing with the results of a global tropospheric chemical transport model and other satellite methods.

5. Validation and Discussion

5.1. Introduction to Validation

[44] In this section, GOME retrievals are validated against other correlative ozone measurements. To reduce the cloud influence, we only use retrievals with cloud

fraction < 0.8 , which removes $\sim 10\%$ of the retrievals. Using a smaller threshold of cloud fraction (e.g., 0.6) gives a slightly worse comparison because of fewer coincidences. For comparisons with TOMS, all gridded TOMS data (~ 10 – 20 points) within a GOME footprint are averaged to make the spatial domain approximately the same. The maximum time difference is ~ 1 hour. The criteria for comparison with DB and ozonesonde measurements are within: (1) 8 hours, (2) $\pm 1.5^{\circ}$ latitude, and (3) 600 km in longitude except at Kaashidhoo, Paramaribo, Kuala Lumpur, and Irene, where the longitude collocation criterion is relaxed to 12° to obtain enough collocations. To reduce the biases due to different surface altitudes, GOME retrievals are adjusted to the same surface altitudes of WUDC stations. The criteria for comparison with SAGE-II data are within: (1) the same day, (2) $\pm 1.5^{\circ}$ latitude, and (3) $\pm 5^{\circ}$ longitude. We first integrate SAGE-II profiles to sub-columns according to GOME retrieval altitude grids and then apply the GOME retrieval AKs to degrade SAGE-II profiles to the GOME vertical resolution. During all the comparisons, we remove outliers which are defined to be outside 3σ of the mean difference for each station. The total numbers of collocations are 4711, 1871, 1989, and 10692 for comparing with TOMS, DB, ozonesonde TCO, and SAGE-II profiles, respectively (Table 1). Table 5 summarizes the Mean Bias (MB), 1σ , and correlation coefficients in TO and TCO between GOME/a priori and correlative measurements.

5.2. Intercomparison of Total Column Ozone (TO)

[45] Figure 8 (left) compares the times series of a priori, retrieved, DB and TOMS TO at selected ozonesonde stations and Figure 8 (right) shows the differences between retrievals and a priori, DB, and TOMS TO. GOME TO agrees very well with TOMS and DB measurements. The retrieved TO values are significantly improved over the a priori values as seen from the much less scattered differences (Figure 8) and much better statistics (Table 5) between retrievals and other TO measurements than between retrievals and their a priori values. There is no clear time-dependent drift in the time series of the differences, suggesting that there is very little degradation in the spectral region of band 2 used during 1996–1999. The MBs between retrieved and TOMS TO are mostly within 6 DU ($< 2\%$) except at a few high-latitude stations, Resolute, Macquarie Island, Marambio, and Neumayer, where the MBs are -10.2 DU (2.5%), -7.8 DU (-2.4%), -9.8 DU (-3.8%), and -6.3 DU (-2.5%), respectively. The SDs are less than 4 DU (1.5%) at stations between 30° S– 30° N and typically less than 6.1 DU (2.4%) at higher latitudes except that the SD at Resolute is 8.7 DU (2.1%). The MBs between GOME and DB TO are mostly within 5 DU (1.5%) except at Resolute, Tateno, Valentia, and Macquarie Island, where the MBs are up to 12 DU (3.3%). However, at Valentia and Tateno, the GOME/TOMS bias is within 2 DU. The SDs range from 3 to 6 DU ($< 3\%$) in the tropics and from 8 to 16 DU ($< 5\%$) at higher latitudes, comparable to those between TOMS and DB TO (not shown in Table 5). Overall, the MBs between GOME and TOMS/DB TO are typically within the retrieval uncertainties of the various measurements.

[46] The spatiotemporal differences between GOME and correlative TO play a large role in leading to the differences

Table 5. Comparison Statistics (Mean Bias in DU, 1σ Standard Deviation in DU, and the Pearson Correlation Coefficient) Between GOME Retrieved/a Priori Total and Tropospheric Column Ozone, and Correlative TOMS, Dobson/Brewer, and Ozonesonde Measurements

Station	Total Column Ozone									Tropospheric Column Ozone					
	GOME-a Priori			GOME-TOMS			GOME-Ground			a Priori-Sonde			GOME-Sonde		
Resolute	-17.6	47.8	0.59	-10.2	8.7	0.99	-12.0	14.9	0.97	5.6	5.7	0.56	0.1	6.2	0.46
Scoresbysund	-10.3	34.5	0.71	1.3	5.0	0.99				2.4	5.4	0.52	-3.3	5.9	0.39
Sodankylä	-25.2	41.9	0.64	-0.5	5.1	1.00	-4.2	11.2	0.98	2.7	3.8	0.62	-0.5	6.5	0.53
Churchill	7.6	25.0	0.81	-0.5	5.0	0.99	0.7	10.7	0.96	3.1	5.2	0.56	1.0	4.2	0.62
Valentia	-23.7	39.2	0.37	1.7	4.4	1.00	-10.1	14.9	0.92	-0.3	8.0	0.27	0.5	6.5	0.25
Hohenpeißenberg	-8.2	29.4	0.66	1.3	4.5	0.99	3.0	10.7	0.95	2.4	5.3	0.59	1.1	5.8	0.56
Payerne	-10.6	29.5	0.65	1.5	4.1	0.99				2.3	5.6	0.64	-0.1	5.6	0.65
Boulder	-5.5	25.1	0.68	5.3	4.2	0.99	3.5	9.2	0.95	3.1	5.7	0.69	1.9	3.9	0.87
Ankara	4.4	21.4	0.84	4.5	3.7	0.99				3.4	4.9	0.83	2.6	5.2	0.87
Wallop Island	-8.5	25.7	0.60	0.6	5.0	0.99	-0.1	9.9	0.94	0.6	6.6	0.69	-3.0	5.4	0.83
Tateno	-2.7	27.9	0.66	0.8	5.3	0.99	6.7	15.7	0.90	3.5	6.6	0.73	0.0	5.2	0.85
Kagoshima	-13.7	20.0	0.67	-1.3	5.0	0.98	2.2	10.8	0.89	6.2	7.6	0.65	1.7	7.8	0.71
Santa Cruz	4.9	16.3	0.50	2.6	4.0	0.97				-4.2	8.2	0.54	1.5	7.4	0.76
Naha	-12.3	14.8	0.72	-0.5	4.0	0.98	1.7	6.1	0.96	6.4	7.0	0.56	5.4	6.1	0.70
Hilo	-5.9	13.1	0.67	-0.7	2.9	0.99	2.3	4.3	0.96	2.6	6.4	0.67	1.7	6.0	0.79
Paramaribo	-5.4	4.9	0.92	-2.7	2.8	0.97				2.0	3.7	0.00	-1.8	3.7	0.22
Kaashidhoo	-4.5	4.1	0.12	-2.5	2.8	0.68				3.4	5.0	0.27	0.9	6.5	0.27
Kuala Lumpur	-4.1	9.8	0.45	-3.9	3.7	0.93				9.0	5.0	0.00	3.0	5.4	0.38
San Cristobal	-7.3	7.2	0.67	-3.6	3.2	0.95				7.8	2.7	0.74	2.7	3.8	0.62
Nairobi	2.4	11.4	0.45	0.1	3.8	0.95	-2.4	4.6	0.89	-1.7	5.9	0.29	-0.7	5.4	0.66
Java	-11.0	7.4	0.71	-3.3	3.4	0.94				4.6	7.5	0.50	-0.1	5.0	0.87
Ascension Island	0.6	7.8	0.67	-1.2	2.3	0.98				-6.9	6.3	0.80	0.0	5.9	0.77
American Samoa	-10.4	8.0	0.60	-3.1	3.0	0.95	2.2	4.2	0.92	5.0	5.8	0.55	1.5	4.5	0.82
Tahiti	-11.5	9.9	0.73	-2.1	3.0	0.98				9.6	5.6	0.47	5.1	4.1	0.82
La Réunion	-8.4	8.3	0.90	-1.4	2.5	0.99				1.6	5.3	0.78	1.8	3.2	0.85
Irene	-11.9	7.5	0.93	-0.9	1.6	0.99	-3.4	7.8	0.96	3.6	5.5	0.79	-0.3	4.6	0.85
Easter Island	-11.3	11.1	0.82	0.3	3.8	0.99				7.2	8.3	0.45	2.6	5.4	0.81
Laverton	-12.0	19.7	0.79	-3.0	3.7	0.99	0.3	5.9	0.97	0.8	3.4	0.68	-2.5	4.7	0.69
Lauder	-9.4	23.4	0.79	-4.2	4.8	0.99	-0.5	6.6	0.99	2.3	3.5	0.62	1.6	4.0	0.40
Macquarie Island	-4.7	26.3	0.75	-7.8	5.5	0.99	-6.7	10.7	0.95	2.6	3.2	0.75	-0.3	5.2	0.56
Marambio	-22.3	45.6	0.26	-9.8	6.1	0.99	4.8	15.4	0.96	-0.7	5.1	0.76	-0.9	5.0	0.81
Syowa	-22.9	39.9	0.80	-3.8	4.8	1.00	-2.3	9.1	0.99	1.0	3.8	0.92	-3.1	5.6	0.80
Neumayer	-25.4	26.6	0.92	-6.3	4.7	1.00				1.7	3.4	0.93	-4.0	5.1	0.89

between various measurements. *Allen and Reck* [1997] found significant daily fluctuations in TO due to planetary- and medium-scale waves; the RMS day-to-day differences are from 2 to 8 DU between $\pm 25^\circ$ and from 5 to 30 DU at midlatitudes. The larger SDs between GOME and TOMS/DB TO at higher latitudes are consistent with the larger TO variability at higher latitudes and also larger retrieval uncertainties of various measurements. The larger SDs between GOME and DB than those between GOME and TOMS are due to the larger spatial domain difference (i.e., $960 \times 80 \text{ km}^2$ area versus point) and the larger temporal collocation criterion (i.e., <8 hours versus ~ 1 hour).

[47] There is a small inter-hemispheric bias between GOME and TOMS TO but not between GOME and DB TO; this is likely from TOMS data. The average biases between GOME and TOMS TO at all the northern and southern hemispheric stations with DB measurements, are -0.4 DU and -4.0 DU, respectively. However, the corresponding biases between GOME and DB TO are -0.6 DU and -1.0 DU. *Labow et al.* [2004] also found this inter-hemispheric bias in the TOMS V8 data relative to DB measurements, with the EP-TOMS/DB bias higher by 1–2% in the southern hemisphere than in the northern hemisphere.

[48] At Resolute, our retrievals are underestimated by 10–12 DU compared to both TOMS and DB measurements. We think that this underestimation is mainly caused by large variation in surface albedo with season and the difficulty in

discriminating between clouds and snow/ice surface in the retrievals. We find large differences in surface albedo of up to 50% between TOMS [*Herman and Celarier*, 1997] and GOME [*Koelemeijer et al.*, 2003] databases at polar regions, supporting that large errors of surface albedo exist.

5.3. Intercomparison of Tropospheric Column Ozone and Tropopause Pressure

[49] Figure 9 (left) compares the time series of a priori, retrieved, and ozonesonde TCO at 7 selected stations, arranged by latitudes. Figure 9 (right) shows corresponding differences of GOME retrievals and a priori relative to ozonesonde TCO. Our retrieved TCO agrees well with ozonesonde measurements at most of the stations and captures most of the temporal variability in ozonesonde TCO. The retrievals agree much better with the ozonesonde measurements than do the a priori values during certain periods at some stations. For example, at the most northern station, Resolute, GOME retrievals agree very well with ozonesonde TCO during the middle of 1997 even though the a priori TCO values are usually higher by 5–15 DU (Figure 9a). The retrieved TCO at Boulder around April of 1996 and 1997 compares better with ozonesonde TCO by up to ~ 10 –15 DU than the a priori values (Figure 9b). At Hilo during the middle of 1997, the ozonesonde TCO varies from ~ 60 DU to 15 DU; our retrievals agree with the ozonesondes, although the a priori TCO values are ~ 25 –

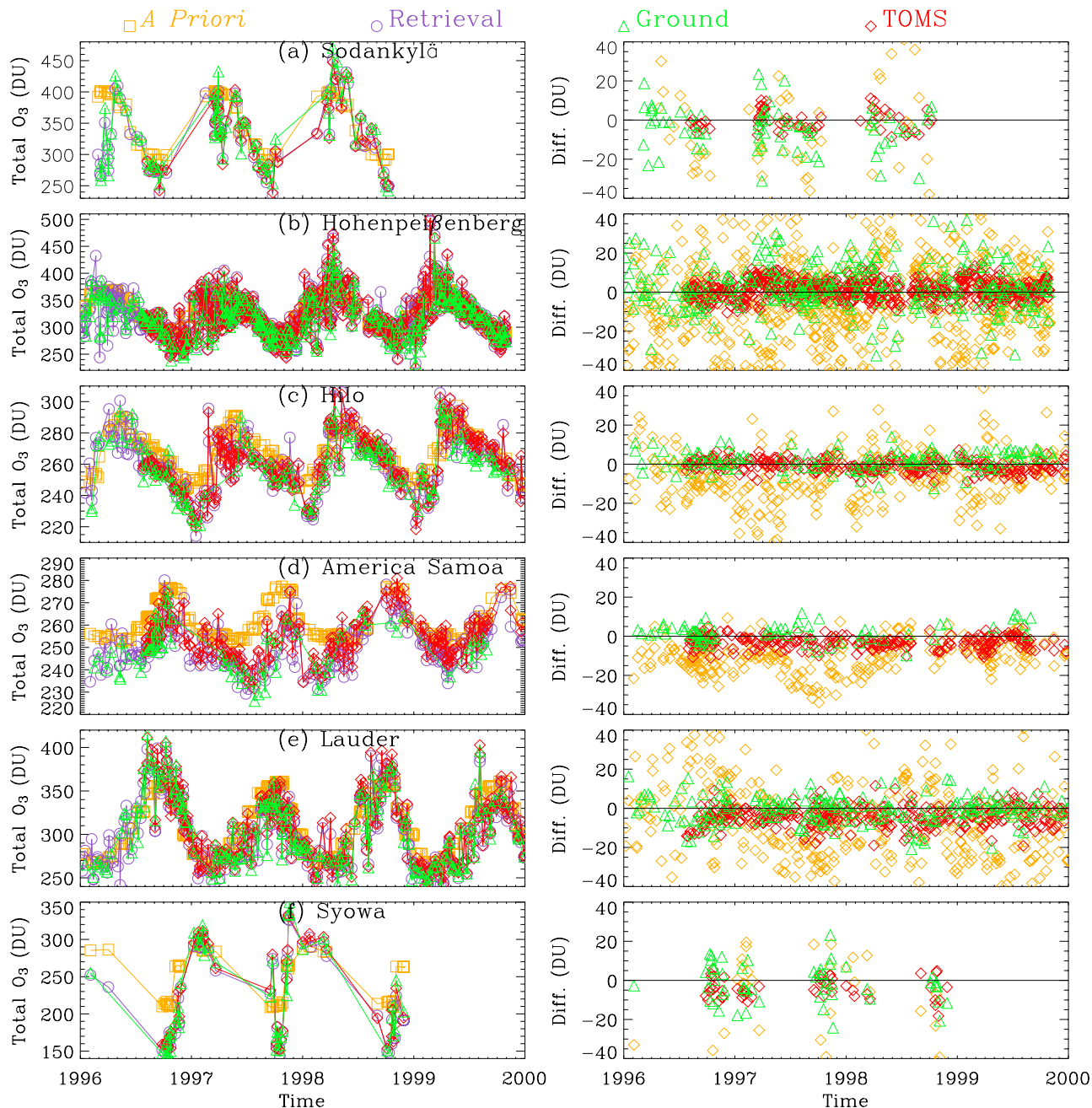


Figure 8. (left) Time series of retrieved (purple), a priori (yellow), ground-based (green), and TOMS (red) total column ozone at seven selected stations. (right) Time series of the differences of retrievals relative to a priori, ground-based, and TOMS total ozone (GOME-others).

35 DU (Figure 9c). Similarly, excellent agreement can be seen at American Samoa during the end of 1997 when the ozonesonde TCO varies from ~ 15 DU to ~ 50 DU (Figure 9f). At Java (Figure 9d), the a priori values are usually around 25–35 DU. However, our retrievals successfully capture the enhanced TCO (>50 DU) during the period of intense biomass burning resulting from the 1997–1998 El Niño event [Thompson *et al.*, 2001; Chandra *et al.*, 2002] as well as some low TCO values (~ 15 –20 DU). At Ascension Island (Figure 9e), the retrievals significantly improve over the a priori values during the biomass burning season. The large improvement over the a priori values demonstrates that the retrieved TCO really comes from the

GOME measurements. We can also see that retrieved TCO with our algorithm is hardly affected by the large instrument degradation after 1998.

[50] The retrievals improve over the a priori values at most of the stations either by reducing the MBs or SDs, or increasing the correlation, or both, except at a few high-latitude stations (Table 5), where the tropospheric ozone information is relatively weak. The MBs between our retrieved and ozonesonde TCO are usually within 3.3 DU ($<15\%$) except at Naha, Tahiti, and Neumayer, where the biases are 5.4 DU (17%), 5.1 DU (26%), and -4.0 DU (-17%), respectively (Table 5). At Resolute, Kagoshima, Kuala Lumpur, San Cristobal, Ascension Island, and Easter

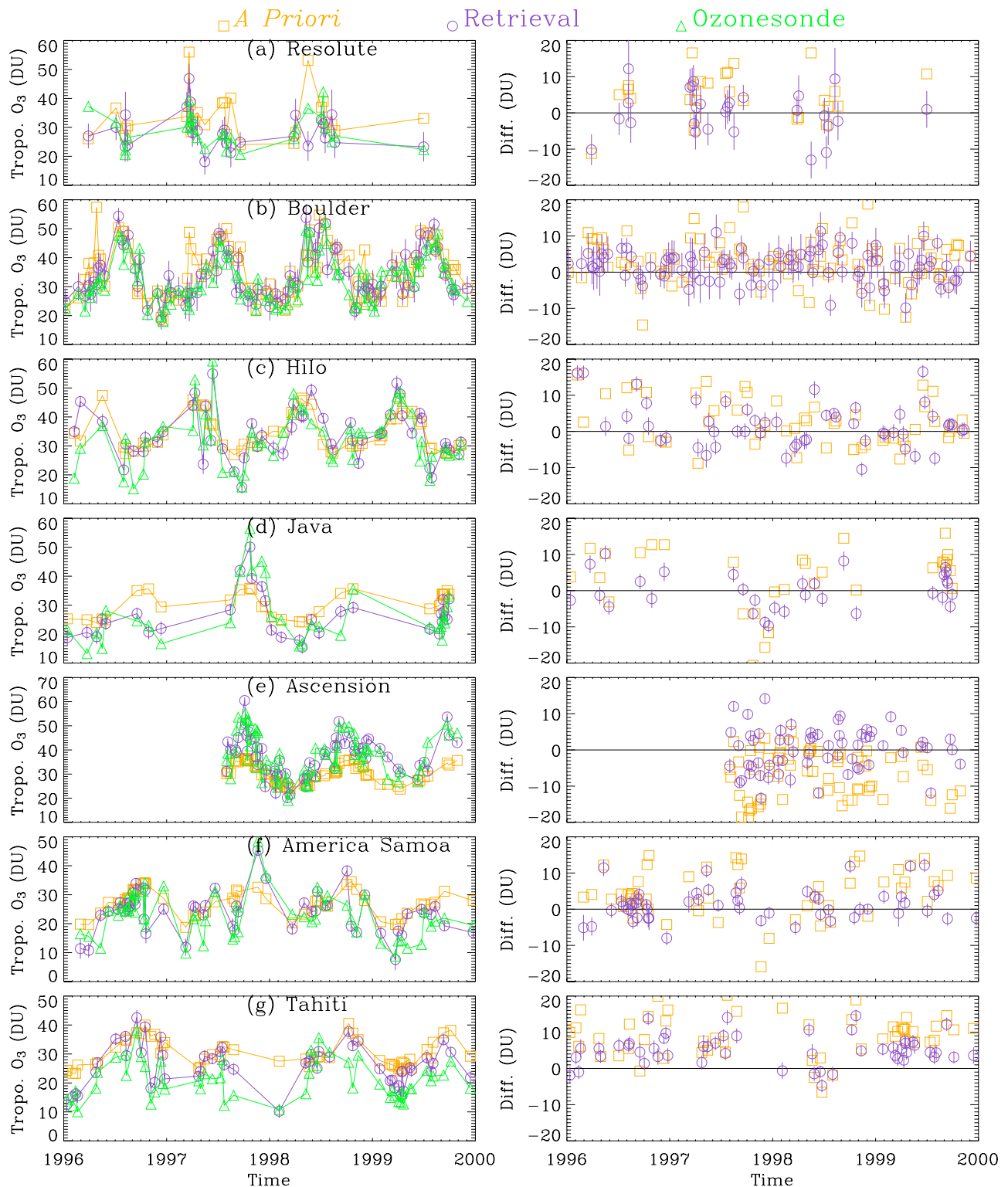


Figure 9. Similar to Figure 8, but for comparisons of Tropospheric Column Ozone (TCO) (retrievals: purple; a priori: yellow; ozonesonde: green). (right) Differences between GOME/a priori and ozonesonde TCO. The error bars indicate the retrieval errors due to smoothing and instrumental random noise in TCO.

Island, the larger a priori biases have been reduced by 4–7 DU in the retrievals. The SDs of the biases range from 3.0 to 8 DU (12–27%). As in the TO comparison, the spatio-temporal variability of TCO can significantly contribute to the observed differences between retrieved and ozonesonde

TCO. *Beekmann et al.* [1994] estimated that the day-to-day variability of tropospheric ozone is $\sim 20\%$ at the Observatoire de Haute Provence in southern France and the spatial variability of free tropospheric ozone is $\sim 20\%$ in Western Europe. SHADOZ observations show that there is consid-

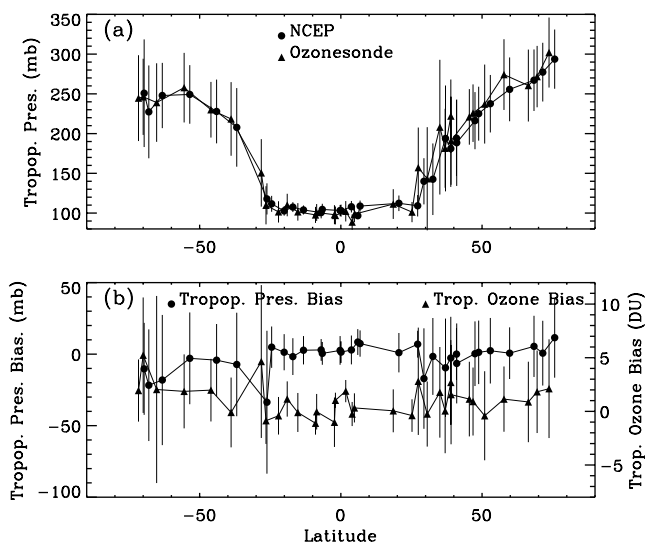


Figure 10. (a) Mean and 1σ standard deviations of NCEP tropopause and ozonesonde tropopause pressure for all the stations. (b) Mean biases and 1σ -standard deviations in tropopause pressure between NCEP and ozonesonde (left axis, circles) and in ozonesonde tropospheric column ozone between using NCEP and ozonesonde tropopause (right axis, triangles).

erable spatiotemporal variability of tropospheric ozone in the tropics [Thompson *et al.*, 2003b].

[51] The retrieved TCO is still affected by the a priori, as shown in Figure 4. For example, the large biases at Tahiti (Figure 9g) are partly due to the fact that the a priori TCO values are too high by ~ 10 DU on average, although some of the biases larger than 14 DU, which cannot be explained by the reduced retrieval sensitivity in the lower troposphere, might be caused by the spatiotemporal variation over this region since the GOME spatial resolution is 960×80 km².

[52] Because the tropopause location is an important source of error for TCO as shown in section 3.6, we evaluate the accuracy of NCEP tropopause with ozonesonde tropopause and assess its effect on TCO. Figure 10a shows both NCEP and ozonesonde tropopause pressure for all the stations and Figure 10b shows their MBs and SDs. We determine ozonesonde tropopause pressure from observed temperature profiles using the WMO definition [WMO, 1957], similar to the NCEP tropopause determination (<http://www.cdc.noaa.gov/PublicData/faq.html>). The NCEP tropopause agrees well with ozonesonde tropopause at most of the stations. The MBs are usually <10 hPa except for a few stations near subtropical jet regions (e.g., Easter Island, Santa Cruz) and at high latitudes. The SDs are <15 hPa in the tropics (30°N – 30°S) and are in the 17–50 hPa range in the extratropics. These SDs are comparable to the actual variability in tropopause pressure (error bars in Figure 10a). Figure 10b also shows the ozonesonde TCO differences and SDs between using NCEP and ozonesonde tropopause. The mean differences are usually <1 DU at most of the stations and are up to 4 DU for those stations with large biases in tropopause. The SDs are <2 DU in the tropics and are usually <4 DU at midlatitudes and high latitudes except for two stations near subtropical jets regions and two southern polar stations. Overall, the NCEP tropopause well represents the

actual thermal tropopause and the errors in TCO due to using NCEP tropopause are within the retrieval uncertainties of TCO at most of the stations. It should be noted that the thermal tropopause may not represent the real stratosphere/troposphere boundary in the extratropics [Hoerling *et al.*, 1991]. However, the errors in our TCO due to the tropopause can be readily corrected by performing interpolation from the retrieved vertical ozone profiles when a superior tropopause (e.g., dynamic tropopause) is available.

5.4. Intercomparison With SAGE-II Ozone Profiles

[53] Figure 11 shows the average differences (thick lines) and 1σ spreads (thin lines) of our retrievals (solid lines) and

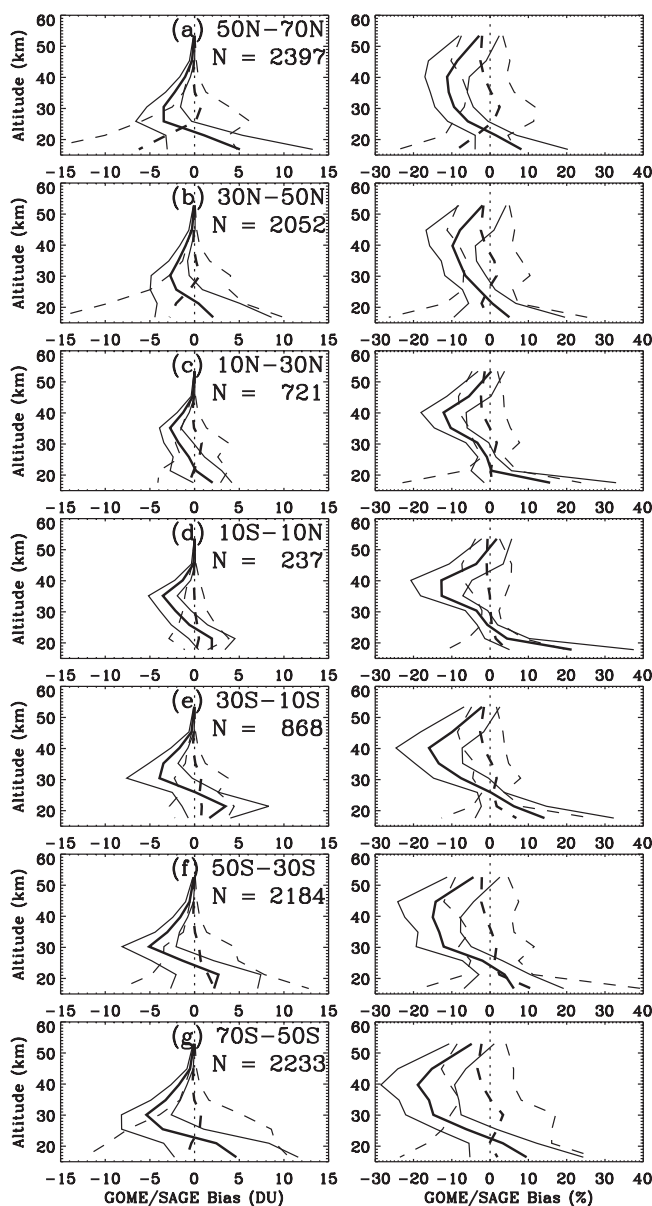


Figure 11. The left panels show the absolute mean bias (thick lines) and 1σ spread (thin lines) between GOME (solid lines)/GOME a priori (dashed lines) and transformed SAGE-II retrievals at seven 20° -latitude bands in 70°N – 70°S . The right panels show relative differences. The number of comparisons (N) is indicated for each latitude band.

a priori (dashed lines) relative to SAGE-II measurements for the top eight layers (~ 15 – 60 km) at seven 20° -latitude bands. The two columns show the absolute and relative biases, respectively. There are systematic biases in our retrievals relative to SAGE-II measurements. The biases are similar at different latitudes, with usually negative biases of <5 DU (15%) for the top five layers and positive biases of <5 DU (15%) for the bottom two layers, although the magnitudes of the biases slightly vary with latitude. The SDs of the biases are within 10% for the top seven layers and within 15% for the bottom layer. The MBs are smaller between a priori and SAGE-II because the a priori values at those altitude ranges are mainly derived from SAGE-II measurements.

[54] Danilin *et al.* [2002] found that SAGE-II ozone is smaller than Improve Limb Atmospheric Spectrometer (ILAS), MLS, and Polar Ozone and Aerosol Measurement II (POAM-II) ozone by 2–8% over altitude range 34–45 km. So GOME ozone is even smaller compared to other data over this altitude range. Wang *et al.* [2002] found that SAGE-II ozone is larger than ozonesonde ozone by $<2\%$ on average over 25–30 km, larger by up to 8% over 18–25 km, and within 10% over 15–18 km. Borchi *et al.* [2005] showed that the SAGE ozone is higher by 2–5% than SAOZ ozone over 19–30 km but smaller by up to 50% over 15–19 km. The above intercomparisons indicate that some of the GOME/SAGE-II biases might arise from SAGE-II data especially below 30 km. However, the altitude-dependent systematic biases with respect to SAGE-II data and those biases of $>10\%$ suggest that systematic errors exist in GOME level-1 data. The negative biases at higher altitudes suggest positive errors in the normalized radiances near 290 nm and positive biases at lower latitudes suggest negative errors near 307 nm. We find that if we do not fit the degradation correction in the retrievals, there are negative biases of up to 30% at high altitudes, suggesting that there is a wavelength-dependent bias in the normalized radiances below 307 nm before applying the degradation correction. After applying the 2nd-order polynomial corrections, such measurement errors are greatly reduced, but there are still some residual measurement errors.

6. Summary

[55] We have developed an algorithm to retrieve ozone profiles including the troposphere from GOME measurements in ultraviolet (289–307 nm, 326–339 nm) using the optimal estimation technique. Tropospheric Column Ozone (TCO) is directly retrieved by using the known tropopause to define the stratosphere/troposphere boundary. With a particular focus on tropospheric ozone retrieval, we perform detailed wavelength and radiometric calibration. The Linearized Discrete Ordinate Radiative Transfer model (LIDORT) is used as the forward model. We further improve the forward modeling by treating the Ring effect directly and performing polarization correction to radiances. We also improve the forward model inputs of clouds, surface albedo and pressure, aerosols, and temperature profiles. The retrieved ozone profiles are best resolved over altitude range of 20–40 km, with vertical resolution of 8–12 km. Significant tropospheric ozone information can be

derived from the measurements. The degrees of freedom for signal in the troposphere range from ~ 1.2 in the tropics to ~ 0.5 at high latitudes. The a priori influence in retrieved TCO ranges from $\sim 15\%$ in the tropics to $\sim 50\%$ at high latitudes. The total errors of the retrievals are estimated to be 20–30% in the troposphere and lower stratosphere and 5–10% in the stratosphere. The globally-average total errors in the retrieved Total column Ozone (TO), Stratospheric Column Ozone (SCO), and TCO are estimated to be 1.6%, 2.3%, 21%, respectively. The dominant sources of errors are the smoothing, instrument random-noise, systematic temperature errors, and errors in cloud-top pressure. Tropopause pressure is also a significant source of error for TCO and SCO and ozone absorption cross section is an important source of error for TO and SCO.

[56] We have validated our retrievals against Dobson/Brewer (DB), Earth-Probe Total Ozone Mapping Spectrometer (TOMS), ozonesonde, and Stratospheric Aerosols and Gas Experiment II (SAGE-II) measurements. The integrated Total column Ozone (TO) agrees with TOMS and DB TO to within retrieval uncertainty of the various techniques and spatiotemporal variability; the Mean Biases (MBs) are typically within 6 DU (2%) and the 1 σ -Standard Deviations (SDs) are within 3–8 DU ($<2.5\%$) versus TOMS and within 3–16 DU ($<5\%$) versus DB. The retrieved TCO captures most of temporal variability in ozonesonde TCO at the majority of ozonesonde stations. The MBs and their SDs are within measurement uncertainties and the TCO variability; the MBs are typically <3 DU (15%) and the SDs are in the 3–8 DU (13–27%) range. The comparison with SAGE-II profiles above ~ 15 km shows MBs and SDs are usually within 15%.

[57] The systematic biases relative to SAGE-II indicate that there are some residual systematic errors in band 1 of GOME level-1 data after the degradation correction. The systematic errors in 313–325 nm are too large to improve the retrievals so that we exclude this region for the present retrievals. If measurements in this spectral region are well calibrated, the quality of the retrieved tropospheric ozone will be further improved. As measurements degrade with time and become noisier, additional degradation corrections will be necessary to keep the same retrieval quality for longer than 10-year GOME record.

[58] Our algorithm can be applied to other nadir-viewing satellite UV measurements, such as those from the GOME-2 instrument, the Scanning Imaging Absorption Spectrometer for Atmospheric Chartography (SCIAMACHY), the Ozone Monitoring Experiment (OMI), and the Ozone Mapping and Profiler Suite (OMPS). The performance, especially for tropospheric ozone, will vary depending on the quality of level-1 data and the spectral resolution.

[59] **Acknowledgments.** This study is supported by the NASA ACPMAP and the Smithsonian Institution. We thank the WOUDC, SHADOZ, CMDL, and their data originators for providing ozonesonde and total ozone data. We thank the TOMS team for the EP-TOMS data and the NASA LRC/LRAB for the SAGE-II data. We thank the NOAA-CIRES CDC for providing NCEP reanalysis data and the ECMWF project for the ERA-40 data. We are grateful to G. Labow for providing the ozone profile climatology and to R. F. van Oss for providing a look-up table for polarization correction. We also thank R. Chatfield, P. I. Palmer, P. K. Bhartia, J. A. Logan, D. J. Jacob, B. J. Johnson, S. J. Oltmans, and two reviewers for their suggestions and comments. We appreciate the ongoing cooperation of the European Space Agency and the German Aerospace Center in the GOME program.

References

- Allen, D. R., and R. A. Reck (1997), Daily variations in TOMS total ozone data, *J. Geophys. Res.*, *102*(D12), 13,603–13,608.
- Basher, R. E. (1982), Review of the Dobson spectrophotometer and its accuracy, Global Ozone Res. and Monit. Proj., World Meteorol. Org., Geneva.
- Bass, A. M., and R. J. Paur (1985), The ultraviolet cross-sections of ozone, I, The measurements, in *Atmospheric Ozone*, edited by C. S. Zerefos and A. Ghazi, pp. 606–610, Springer, New York.
- Bates, D. R. (1984), Rayleigh scattering by air, *Planet. Space Sci.*, *32*, 785–799.
- Bauman, J. J., P. B. Russell, M. A. Geller, and P. Hamill (2003), Stratospheric aerosol climatology from SAGE II and CLAES measurements: 2. Results and comparisons, 1984–1999, *J. Geophys. Res.*, *108*(D13), 4383, doi:10.1029/2002JD002993.
- Beckmann, M., G. Ancellet, and G. Megie (1994), Climatology of tropospheric ozone in the southern Europe and its relation to potential vorticity, *J. Geophys. Res.*, *99*(D6), 12,841–12,853.
- Bhartia, P. K., and C. G. Wellemeyer (2002), TOMS-V8 total ozone algorithm, in *OMI Algorithm Theoretical Basis Document*, edited by P. K. Bhartia, NASA Goddard Space Flight Cent., Greenbelt, Md.
- Bhartia, P. K., R. D. McPeters, C. L. Mateer, L. E. Flynn, and C. Wellemeyer (1996), Algorithm for the estimation of vertical ozone profiles from the backscattered ultraviolet technique, *J. Geophys. Res.*, *101*(D13), 18,793–18,806.
- Bodhaine, B. A., N. B. Wood, E. G. Dutton, and J. R. Slusser (1999), On Rayleigh optical depth calculations, *J. Atmos. Oceanic Technol.*, *16*, 1854–1866.
- Bogumil, K., et al. (2003), Measurements of molecular absorption spectra with the SCIAMACHY pre-flight model: Instrument characterization and reference data for atmospheric remote-sensing in the 230–2380 nm region, *J. Photoch. Photobiol. A.*, *157*(2–3), 167–184.
- Borchi, F., J.-P. Pommereau, A. Garnier, and M. Pinharanda (2005), Evaluation of SHADOZ sondes, HALOE and SAGE II ozone profiles at the tropics from SAOZ UV-Vis remote measurements onboard long duration balloons, *Atmos. Chem. Phys.*, *5*, 1381–1397.
- Brion, J., A. Chakir, D. Daumont, and J. Malicet (1993), High-resolution laboratory absorption cross section of O₃. Temperature effect, *Chem. Phys. Lett.*, *213*(5–6), 610–612.
- Burrows, J. P., A. Dehn, B. Deters, S. Himmelmann, A. Richter, S. Voigt, and J. Orphal (1999), Atmospheric remote-sensing reference data from GOME: Part 2. Temperature-dependent absorption cross-sections of O₃ in the 231–794 nm range, *J. Quant. Radiat. Transfer*, *61*(6), 509–517.
- Caudill, T. R., D. E. Flittner, B. M. Herman, O. Torres, and R. D. McPeters (1997), Evaluation of the pseudo-spherical approximation for backscattered ultraviolet radiances and ozone retrieval, *J. Geophys. Res.*, *102*(D3), 3881–3890.
- Chance, K. (1998), Analysis of BrO measurements from the global ozone monitoring experiment, *Geophys. Res. Lett.*, *25*(17), 3335–3338.
- Chance, K. V., and R. J. D. Spurr (1997), Ring effect studies: Rayleigh scattering, including molecular parameters for rotational Raman scattering, and the Fraunhofer spectrum, *Appl. Opt.*, *36*(21), 5224–5230.
- Chance, K. V., J. P. Burrows, D. Perner, and W. Schneider (1997), Satellite measurements of atmospheric ozone profiles, including tropospheric ozone, from ultraviolet/visible measurements in the nadir geometry: A potential method to retrieve tropospheric ozone, *J. Quant. Spectrosc. Radiat. Transfer*, *57*(4), 467–476.
- Chandra, S., J. R. Ziemke, P. K. Bhartia, and R. V. Martin (2002), Tropical tropospheric ozone: Implications for dynamics and biomass burning, *J. Geophys. Res.*, *107*(D14), 4188, doi:10.1029/2001JD000447.
- Chandra, S., J. R. Ziemke, and R. V. Martin (2003), Tropospheric ozone at tropical and middle latitudes derived from TOMS/MLS residual: Comparison with a global model, *J. Geophys. Res.*, *108*(D9), 4291, doi:10.1029/2002JD002912.
- Chin, M., et al. (2002), Tropospheric aerosol optical thickness from the GOCART model and comparisons with satellite and sunphotometer measurements, *J. Atmos. Sci.*, *59*, 461–483.
- Danilin, M. Y., et al. (2002), Trajectory hunting as an effective technique to validate multiplatform measurements: Analysis of the MLS, HALOE, SAGE-II, ILAS, and POAM-II data in October–November 1996, *J. Geophys. Res.*, *107*(D20), 4420, doi:10.1029/2001JD002012.
- DLR (2002), GOME level 0 to 1 algorithms description, Oberpfaffenhofen, Germany.
- European Space Agency (ESA) (1995), The GOME Users Manual, *ESA Publ. SP-1182*, Publ. Div., Eur. Space Res. and Technol. Cent., Noordwijk, Netherlands.
- Fujiwara, M., K. Kita, T. Ogawa, S. Kawakami, T. Sano, N. Komala, S. Saraspriya, and A. Suropto (2000), Seasonal variation of tropospheric ozone in Indonesia revealed by 5-year ground-based observations, *J. Geophys. Res.*, *105*(D2), 1879–1888.
- Goldman, S. (1953), *Information Theory*, Prentice-Hall, New York.
- Hasekamp, O. P., and J. Landgraf (2001), Ozone profile retrieval from backscattered ultraviolet radiances: The inverse problem solved by regularization, *J. Geophys. Res.*, *106*(D8), 8077–8088.
- Herman, J. R., and E. A. Celarier (1997), Earth surface reflectivity climatology at 340–380 nm from TOMS data, *J. Geophys. Res.*, *102*(D23), 28,003–28,011.
- Hoerling, M. P., T. K. Schaack, and A. J. Lenzen (1991), Global objective tropopause analysis, *Mon. Weather Rev.*, *119*(8), 1816–1831.
- Hoogen, R., V. V. Rozanov, and J. P. Burrows (1999), Ozone profiles from GOME satellite data: Algorithm description and first validation, *J. Geophys. Res.*, *104*(D7), 8263–8280.
- Hsu, N. C., R. D. McPeters, C. J. Seftor, and A. M. Thompson (1997), Effect of an improved cloud climatology on the total ozone mapping spectrometer total ozone retrieval, *J. Geophys. Res.*, *102*(D4), 4247–4255.
- Hudson, R. D., J.-H. Kim, and A. M. Thompson (1995), On the derivation of tropospheric column from radiances measured by the Total Ozone Mapping Spectrometer, *J. Geophys. Res.*, *100*, 11,137–11,145.
- Kerr, J. B., and C. T. McElroy (1995), Total ozone measurements made with the Brewer ozone spectrophotometer during STOIC 1989, *J. Geophys. Res.*, *100*, 9225–9230.
- Kerr, J. B., I. A. Asbridge, and W. F. J. Evans (1988), Intercomparison of total ozone measured by the Brewer and Dobson spectrophotometers at Toronto, *J. Geophys. Res.*, *93*(D9), 11,129–11,140.
- Koelemeijer, R. B. A., and P. Stammes (1999), Effects of clouds on ozone column retrieval from GOME UV measurements, *J. Geophys. Res.*, *104*(D7), 8281–8294.
- Koelemeijer, R. B. A., J. F. d. Haan, and P. Stammes (2003), A database of spectral surface reflectivity in the range 335–772 nm derived from 5.5 years of GOME observations, *J. Geophys. Res.*, *108*(D2), 4070, doi:10.1029/2002JD002429.
- Kurosu, T. P., K. Chance, and R. J. D. Spurr (1998), Cloud retrieval algorithm for the European Space Agency's Global Ozone Monitoring Experiment, in *Proceedings of SPIE, EUROPTO Series: Satellite Remote Sensing of Clouds and the Atmosphere III*, vol. 495, edited by J. E. Russel, pp. 17–26, SPIE—The Int. Soc. for Opt. Eng., Bellingham, Wash.
- Labow, G. J., R. D. McPeters, and P. K. Bhartia (2004), A comparison of TOMS and SBUV version 8 total column ozone data with data from ground stations, in *Proceedings of the XX Quadrennial Ozone Symposium*, edited by C. S. Zerefos, pp. 123–124, Kos, Greece.
- Latter, B. G., B. Kerridge, and R. Siddans (2003), RAL GOME scan mirror degradation correction, paper presented at 4th Meeting of GOME Ozone Profile Retrieval Working Group, Frascati, Italy.
- Liu, X., M. J. Newchurch, and J. H. Kim (2003), Occurrence of ozone anomalies over cloudy areas in TOMS version-7 level-2 data, *Atmos. Chem. Phys.*, *3*, 1113–1129.
- Liu, X., M. J. Newchurch, R. Loughman, and P. K. Bhartia (2004), Errors resulting from assuming opaque Lambertian clouds in TOMS ozone retrieval, *J. Quant. Spectrosc. Radiat. Transfer*, *85*, 337–365.
- Martin, R. V., D. J. Jacob, R. M. Yantosca, M. Chin, and P. Ginoux (2003), Global and regional decreases in tropospheric oxidants from photochemical effects of aerosols, *J. Geophys. Res.*, *108*(D3), 4097, doi:10.1029/2002JD002622.
- McPeters, R. D., J. A. Logan, and G. J. Labow (2003), Ozone climatological profiles for version 8 TOMS and SBUV retrievals, *Eos. Trans. AGU*, *84*(46), Fall Meet. Suppl., Abstract A21D-0998.
- Mishchenko, M. I., A. A. Lacis, and L. D. Travis (1994), Errors induced by the neglect of polarization in radiance calculations for Rayleigh scattering atmospheres, *J. Quant. Spectrosc. Radiat. Transfer*, *51*, 491–510.
- Müller, M. D., A. K. Kaifel, M. Weber, S. Tellmann, J. P. Burrows, and D. Loyola (2003), Ozone profile retrieval from Global Ozone Monitoring Experiment (GOME) data using a neural network approach (Neural Network Ozone Retrieval System (NNORSY)), *J. Geophys. Res.*, *108*(D16), 4497, doi:10.1029/2002JD002784.
- Munro, R., R. Siddans, W. J. Reburn, and B. Kerridge (1998), Direct measurement of tropospheric ozone from space, *Nature*, *392*, 168–171.
- Newchurch, M. J., X. Liu, J. H. Kim, and P. K. Bhartia (2001), On the accuracy of TOMS retrievals over cloudy regions, *J. Geophys. Res.*, *106*(D23), 32,315–32,326.
- Orphal, J. (2003), A critical review of the absorption cross-sections of O₃ and NO₂ in the 240–790 nm region, *J. Photochem. Photobiol. A.*, *157*, 185–209.
- Rodgers, C. D. (2000), *Inverse Methods for Atmospheric Sounding: Theory and Practice*, World Sci., Hackensack, N. J.

- Schutgens, N. A. J., and P. Stammes (2003), A novel approach to the polarization correction of spaceborne spectroscopy, *J. Geophys. Res.*, *108*(D7), 4229, doi:10.1029/2002JD002736.
- Siddans, R. (2003), Height-resolved ozone retrievals from Global Ozone Monitoring Experiment, Ph.D. dissertation thesis, Univ. of Reading, Chilton, Didcot, UK.
- Sioris, C. E., and W. F. J. Evans (2000), Impact of rotational Raman scattering in the O₂ A band, *Geophys. Res. Lett.*, *27*(24), 4085–4088.
- Spurr, R. J. D. (2002), Simultaneous derivation of intensities and weighting functions in a general pseudo-spherical discrete ordinate radiative transfer treatment, *J. Quant. Spectrosc. Radiat. Transfer*, *75*, 129–175.
- Spurr, R. J. D., T. P. Kurosu, and K. V. Chance (2001), A linearized discrete ordinate radiative transfer model for atmospheric remote-sensing retrieval, *J. Quant. Spectrosc. Radiat. Transfer*, *68*, 689–735.
- Thompson, A. M., D. P. McNamara, K. E. Pickering, and R. D. McPeters (1993), Effect of marine stratocumulus on TOMS ozone, *J. Geophys. Res.*, *98*, 23,051–23,057.
- Thompson, A. M., J. C. Witte, R. D. Hudson, H. Guo, J. R. Herman, and M. Fujiwara (2001), Tropical tropospheric ozone and biomass burning, *Science*, *291*, 2128–2132.
- Thompson, A. M., et al. (2003a), Southern Hemisphere Additional Ozone-sondes (SHADOZ) 1998–2000 tropical ozone climatology: 1. Comparison with Total Ozone Mapping Spectrometer (TOMS) and ground-based measurements, *J. Geophys. Res.*, *108*(D2), 8238, doi:10.1029/2001JD000967.
- Thompson, A. M., et al. (2003b), Southern Hemisphere Additional Ozone-sondes (SHADOZ) 1998–2000 tropical ozone climatology: 2. Tropospheric variability and the zonal wave-one, *J. Geophys. Res.*, *108*(D2), 8241, doi:10.1029/2002JD002241.
- Torres, O., and P. K. Bhartia (1999), Impact of tropospheric aerosol absorption on ozone retrieval from backscattered ultraviolet measurements, *J. Geophys. Res.*, *104*(D17), 21,569–21,577.
- Vandaele, A. C., C. Hermans, S. Fally, M. Carleer, M.-F. Merienne, A. Jenouvrier, B. Coquart, and R. Colin (2003), Absorption cross-sections of NO₂: Simulation of temperature and pressure effects, *J. Quant. Spectrosc. Radiat. Transfer*, *76*, 373–391.
- van der A, R. J., R. F. van Oss, A. J. M. Pijters, J. P. F. Fortuin, Y. J. Meijer, and H. M. Kelder (2002), Ozone profile retrieval from recalibrated GOME data, *J. Geophys. Res.*, *107*(D15), 4239, doi:10.1029/2001JD000696.
- van Oss, R. F., and R. J. D. Spurr (2002), Fast and accurate 4 and 6 stream linearized discrete ordinate radiative transfer models for ozone profile retrieval, *J. Quant. Spectrosc. Radiat. Transfer*, *75*, 177–220.
- van Oss, R. F., R. H. M. Voors, and R. J. D. Spurr (2001), Ozone profile algorithm, in *OMI Algorithm Theoretical Basis Document*, vol. 2, *OMI Ozone Products*, edited by P. K. Bhartia, pp. 51–73, NASA Goddard Space Flight Cent., Greenbelt, Md.
- Vountas, M., V. V. Rozanov, and J. P. Burrows (1998), Ring effect: impact of rotational Raman scattering on radiative transfer in earth's atmosphere, *J. Quant. Spectrosc. Radiat. Transfer*, *60*(6), 943–961.
- Wang, H. J., D. M. Cunnold, L. W. Thomason, J. M. Zawodny, and G. E. Bodeker (2002), Assessment of SAGE version 6.1 ozone data quality, *J. Geophys. Res.*, *107*(D23), 4691, doi:10.1029/2002JD002418.
- Wilmouth, D. M., T. F. Hanisco, N. M. Donahue, and J. G. Anderson (1999), Fourier transform ultraviolet spectroscopy of the A²Π_{3/2}-X²Π_{3/2} Transition of BrO, *J. Phys. Chem. A.*, *103*(45), 8935–8945.
- World Meteorological Organization (WMO) (1957), Definition of the tropopause, *WMO Bull.*, *6*, 136.
- World Meteorological Organization (WMO) (1998), SPARC/IO3C/GAW assessment of trends in the vertical distribution of ozone, *Rep. 43*, Global Ozone Res. and Monit. Proj., Geneva.

K. Chance, T. P. Kurosu, X. Liu, R. V. Martin, C. E. Sioris, and R. J. D. Spurr, Atomic and Molecular Physics Division, Harvard-Smithsonian Center for Astrophysics, Cambridge, MA 02138, USA. (xliu@cfa.harvard.edu)

M. J. Newchurch, Atmospheric Science Department, University of Alabama, Huntsville, AL 35805, USA.